

Component masses of young, wide, non-magnetic white dwarf binaries in the Sloan Digital Sky Survey Data Release 7

R. B. Baxter,^{1★} P. D. Dobbie,^{2★} Q. A. Parker,^{1,3,4} S. L. Casewell,⁵ N. Lodieu,^{6,7}
M. R. Burleigh,⁵ K. A. Lawrie,⁵ B. Külebi,⁸ D. Koester⁹ and B. R. Holland²

¹*Department of Physics & Astronomy, Macquarie University, NSW 2109, Australia*

²*School of Physical Sciences, University of Tasmania, Hobart, TAS 7001, Australia*

³*Macquarie Research Center for Astronomy, Astrophysics & Astrophotonics, Macquarie University, NSW 2109, Australia*

⁴*Australian Astronomical Observatory, PO Box 296, Epping, NSW 1710, Australia*

⁵*Department of Physics & Astronomy, University of Leicester, Leicester LE1 7RH, UK*

⁶*Instituto de Astrofísica de Canarias, Via Lactea s/n, E-38200 La Laguna, Tenerife, Spain*

⁷*Departamento de Astrofísica, Universidad de La Laguna (ULL), E-38206 La Laguna, Tenerife, Spain*

⁸*Institut de Ciències de l'Espai (CSIC-IEEC), Facultat de Ciències, Campus UAB, Torre C5-parell, 2^a planta, E-08193 Bellaterra, Spain*

⁹*Institut für Theoretische Physik und Astrophysik, Christian-Albrechts-Universität, D-24098 Kiel, Germany*

Accepted 2014 March 6. Received 2014 March 2; in original form 2014 January 24

ABSTRACT

We present a spectroscopic component analysis of 18 candidate young, wide, non-magnetic, double-degenerate binaries identified from a search of the Sloan Digital Sky Survey Data Release 7 (DR7). All but two pairings are likely to be physical systems. We show SDSS J084952.47+471247.7 + SDSS J084952.87+471249.4 to be a wide DA + DB binary, only the second identified to date. Combining our measurements for the components of 16 new binaries with results for three similar, previously known systems within the DR7, we have constructed a mass distribution for the largest sample to date (38) of white dwarfs in young, wide, non-magnetic, double-degenerate pairings. This is broadly similar in form to that of the isolated field population with a substantial peak around $M \sim 0.6 M_{\odot}$. We identify an excess of ultramassive white dwarfs and attribute this to the primordial separation distribution of their progenitor systems peaking at relatively larger values and the greater expansion of their binary orbits during the final stages of stellar evolution. We exploit this mass distribution to probe the origins of unusual types of degenerates, confirming a mild preference for the progenitor systems of high-field-magnetic white dwarfs, at least within these binaries, to be associated with early-type stars. Additionally, we consider the 19 systems in the context of the stellar initial mass–final mass relation. None appear to be strongly discordant with current understanding of this relationship.

Key words: binaries: general – stars: magnetic field – white dwarfs.

1 INTRODUCTION

A substantial proportion of stars reside in binary or multiple stellar systems (e.g. Duquennoy & Mayor 1991; Fischer & Marcy 1992; Kouwenhoven et al. 2005, 2007). Empirical determinations of the stellar binary fraction as a function of primary mass and of the binary mass ratio and orbital period distributions inform theories of the star formation process (e.g. Zinnecker 1984; Pinfield et al. 2003; Parker & Reggiani 2013). Moreover, studies of close systems, with orbital periods of a few days or less, can yield important dynamical determinations of masses and radii which lend themselves to arguably

the most stringent examinations of models of stellar structure (e.g. Huang & Struve 1956; Maxted et al. 2004; Clausen et al. 2008). Wide, spatially resolved, binary systems, where the components are separated by 100–10 000 au and have generally evolved essentially as single stars (e.g. Andrews et al. 2012), are also of significant interest, since they are, in effect, miniature versions of open clusters, the traditional but often rather distant testbeds for refining our theories of stellar evolution (e.g. Barbaro & Pigatto 1984; Nordstroem, Andersen & Andersen 1996; Casewell et al. 2009, 2012; Kalirai & Richer 2010).

By considering observational constraints on the stellar binary fraction across a broad range of primary masses, from the late-F/G stars (57 per cent; Duquennoy & Mayor 1991) to the numerically dominant low-mass M dwarfs (26 per cent; Delfosse et al. 2004),

* E-mail: richardbrucebaxter@gmail.com

Lada (2006) has highlighted that the majority of stars reside in single stellar systems. However, since only those stars of the Galactic disc with $M \gtrsim 1 M_{\odot}$ have had sufficient time to evolve beyond the main sequence, around half or more of the members of the field white dwarf population presumably must have once been part of multiple systems. Miszalski et al. (2009) determine that around at least 12–21 per cent of planetary nebulae have close binary central stars, while Holberg et al. (2008, 2013) have concluded that at least 25–30 per cent of the white dwarfs within 20 pc of the Sun are presently part of binary systems, with around 6 per cent being double-degenerates. The systems at the short end of the double-degenerate period distribution are of substantial astrophysical relevance since a subset may ultimately evolve to Type Ia supernovae (e.g. Yoon, Podsiadlowski & Rosswog 2007). Widely separated double-degenerates are also of interest for setting limits on the age of the Galactic disc through the white dwarf luminosity function (Oswalt et al. 1996) and for investigating the late stages of stellar evolution, in particular the heavy mass-loss experienced on the asymptotic giant branch, as manifest through the form of the stellar initial mass–final mass relation (IFMR; e.g. Finley & Koester 1997). Additionally, when a wide double-degenerate harbours an unusual or peculiar white dwarf (e.g. a high-field-magnetic white dwarf), measurements of the parameters of the normal component can be used to investigate its fundamental parameters and origins, either directly or potentially statistically (e.g. Girven et al. 2010; Dobbie et al. 2012a, 2013).

Here, we begin to build the foundations for a statistical approach by presenting the mass distribution for what is by far the largest spectroscopically observed sample (38) of non-magnetic white dwarfs residing in young, wide, double-degenerate systems, to date. In subsequent sections, we describe our photometric identification of 53 candidate young, wide, binary systems from a search of the Sloan Digital Sky Survey (SDSS) data release 7 (DR7; Abazajian et al. 2009) and discuss our new spectroscopic follow-up and analysis of the components of 18 of these systems and detail our assessment of their physical reality. We assemble a mass distribution for the components of the systems we find to have a strong likelihood of being binaries and those of three previously identified wide double-degenerates within the DR7 footprint. We compare this to that of isolated field white dwarfs and discuss the similarities and the differences. We demonstrate how this mass distribution can be used to probe the origins of unusual degenerates, in this case high-field-magnetic white dwarfs (HFMDWs). Finally, we explore the 19 non-magnetic binary systems within the context of our current understanding of the form of the stellar IFMR.

2 THE INITIAL SELECTION OF CANDIDATE YOUNG, WIDE, DOUBLE-DEGENERATES FROM THE SDSS DR7

An initial search for candidate, young, wide, white dwarf + white dwarf binaries was conducted using photometry obtained from the SDSS DR7 data base (e.g. Baxter 2011). The SDSS is a deep, wide-area, five band [u (3551 Å), g (4686 Å), r (6165 Å), i (7481 Å) and z (8931 Å)] imaging survey of the night sky that is supplemented by fibre spectroscopic follow-up of select sources (e.g. quasars). A comprehensive description of this impressively large project can be found in York et al. (2000), while full details of the DR7, which is of particular relevance to this work, are provided by Abazajian et al. (2009). In brief, the 7th data release includes imaging for an area of 11 663 square degrees (a substantial proportion of which is centred on the northern Galactic cap) and catalogues 357 million

unique sources down to 5σ photometric limits at u , g , r and i of 22.3, 23.3, 23.1 and 22.3 mag., respectively. The imaging was acquired with a drift scan technique in seeing of better than 1.5 arcsec, so the median full width at half-maximum of the point spread function is approximately 1.4 arcsec at r . The re-constructed SDSS images have pixels which are 0.396 arcsec on a side.

As is evident from fig. 1 of Harris et al. (2003), the photometric band passes of the SDSS and the colours which can be derived from them are rather effective at discriminating hot ($T_{\text{eff}} > 8000\text{--}9000\text{ K}$), generally young, white dwarfs from the bulk of the field main-sequence stars which dominate colour–magnitude and colour–colour diagrams. We selected from DR7 (using an SQL query) all point sources flagged as photometrically clean with $r \leq 20.0$, $u - g > -0.7$, $u - g \leq 0.5$, $g - r > -0.7$, $g - r \leq 0.0$ and $r - i < 0.0$, which have another object satisfying these colour and magnitude criteria within 30 arcsec. In drawing up these criteria, we crudely appraised the likely contribution of chance stellar alignments to our sample of candidate binaries. We compared the cumulative number of observed pairings with separations of less than 60 arcsec to that predicted for a random on-sky distribution of objects by equation (1) (Struve 1852), where N is the number of sources satisfying the photometric selection criteria ($N = 36\,231$) in area A (square degrees, $A = 11\,663$) and ρ is the maximum projected separation (degrees),

$$n(\leq \rho) = N(N - 1)\pi\rho^2/2A. \quad (1)$$

On this basis, we anticipate approximately 90 per cent of the pairings with separations of less than 30 arcsec to be physical systems (Fig. 1), although we note our estimate neglects the variations of Galactic latitude within the sample and that a sizeable proportion of sources around $u - g = 0.0\text{--}0.5$, $g - r = -0.2\text{--}0.0$ are likely to be quasars. Additionally, we considered that the atmospheres of cooler white dwarfs (i.e. $T_{\text{eff}} \lesssim 8000\text{ K}$) are significantly more difficult to model reliably due to the emergence of more physically complex sources of opacity (Koester 2010). Moreover, by restricting our sample to relatively conservative faint magnitude limits, we maintain the advantage that our sources can be followed-up spectroscopically on an 8 m class telescope in reasonable integration times

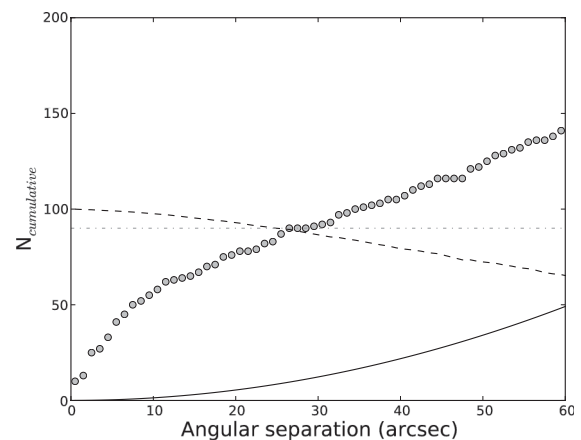


Figure 1. A plot of the cumulative number of observed pairings that meet our photometric selection criteria (filled grey circles) and are expected for a random on-sky distribution of objects (black line) as a function of angular separation. A crude estimate of the proportion of physical systems as a function of angular separation is also shown (dashed line). For angular separations of 30 arcsec or less, roughly 90 per cent of candidates are likely to be physical binaries.

(e.g. about 15 min in photometric conditions, or 2 h in poor weather conditions).

The resulting 91 candidate systems were visually inspected using the SDSS finder chart tool to weed out a substantial number of spurious pairings attributable to blue point-like detections within nearby galaxies, which our contamination estimate above does not account for. To identify further potential contaminants, we also

cross correlated our candidates against the SDSS DR7 quasar list of Schneider et al. (2010). Our cleaned sample includes 53 candidate systems and recovers the three previously known double-degenerate binaries, PG 0922+162 (Finley & Koester 1997), HS 2240+1234 (Jordan et al. 1998) and WD 222301.62+220131.3 (Koester et al. 2009) within the DR7 footprint. Details of all 53 candidates are listed in Table 1.

Table 1. Survey designation, SDSS designation, photometric data and observed angular separations for the candidate double-degenerate systems (CDDS) we have identified. Candidates for which we have obtained new resolved spectroscopy (Spec follow-up = Y) and objects for which a spectroscopic analysis exists in the literature (Spec follow-up = L) are labelled. White dwarfs included in Baxter (2011) (B) and those with SDSS DR7 spectroscopy (italics) are also highlighted.

CDDS ID (Desig.)	SDSS (Desig.)	Spec follow-up	<i>u</i> (mag)	<i>g</i> (mag)	<i>r</i> (mag)	<i>i</i> (mag)	SDSS (Desig.)	<i>u</i> (mag)	<i>g</i> (mag)	<i>r</i> (mag)	<i>i</i> (mag)	Sep. (arcsec)
CDDS1	J000142.84+251506.1		17.81(0.02)	17.79(0.02)	18.16(0.02)	18.45(0.02)	<i>J000142.79+251504.0</i>	19.16(0.19)	18.70(0.16)	19.01(0.16)	19.32(0.17)	2.16
CDDS2	J002925.28+001559.7		20.02(0.05)	19.59(0.02)	19.59(0.02)	19.68(0.02)	<i>J002925.62+001552.7</i>	18.91(0.03)	18.48(0.01)	18.53(0.02)	18.65(0.02)	8.64
CDDS3 ^B	J005212.26+135302.0	Y	17.79(0.02)	17.71(0.03)	17.98(0.02)	18.24(0.02)	J005212.73+135301.1	19.35(0.03)	18.89(0.03)	18.92(0.02)	19.05(0.02)	6.78
CDDS4	<i>J011714.48+244021.5</i>		19.94(0.03)	19.63(0.02)	19.77(0.02)	20.06(0.03)	J011714.12+244020.3	20.29(0.04)	19.83(0.02)	19.96(0.02)	20.16(0.03)	5.05
CDDS5	J012726.89+391503.3		19.16(0.03)	18.70(0.02)	18.83(0.02)	19.01(0.02)	J012725.51+391459.2	20.35(0.06)	19.99(0.02)	19.99(0.02)	20.07(0.03)	16.55
CDDS6 ^B	J021131.51+171430.4	Y	17.36(0.12)	17.26(0.09)	17.65(0.07)	17.87(0.08)	J021131.52+171428.3	16.60(0.02)	16.71(0.02)	17.08(0.01)	17.40(0.01)	2.04
CDDS7	<i>J022733.09+005200.3</i>		20.03(0.05)	19.62(0.02)	19.69(0.02)	19.80(0.03)	<i>J022733.15+005153.6</i>	20.30(0.06)	19.86(0.02)	19.91(0.02)	19.99(0.03)	6.72
CDDS8 ^B	<i>J033236.86-004936.9</i>	Y	15.32(0.01)	15.64(0.02)	16.09(0.02)	16.41(0.02)	<i>J033236.60-004918.4</i>	18.64(0.03)	18.20(0.02)	18.30(0.02)	18.45(0.02)	18.91
CDDS9	J054519.81+302754.0	Y	20.19(0.05)	19.82(0.02)	19.96(0.02)	20.10(0.03)	J054518.98+302749.3	20.05(0.05)	19.64(0.02)	19.80(0.02)	19.97(0.03)	11.72
CDDS10	<i>J072147.38+322824.1</i>		18.18(0.02)	18.07(0.01)	18.17(0.01)	18.28(0.01)	J072147.20+322822.4	18.76(0.08)	18.32(0.06)	18.34(0.06)	18.44(0.06)	2.77
CDDS11 ^{D2}	<i>J074853.07+302543.5</i>	Y	17.41(0.07)	17.59(0.05)	17.88(0.05)	18.49(0.12)	<i>J074852.95+302543.4</i>	17.57(0.05)	17.59(0.04)	17.96(0.04)	18.24(0.03)	1.50
CDDS12	J075410.53+123947.3		19.19(0.09)	18.78(0.06)	18.99(0.08)	19.22(0.07)	J075410.58+123945.5	19.22(0.04)	18.86(0.05)	18.99(0.04)	19.25(0.04)	2.00
CDDS13	<i>J080212.54+242043.6</i>		19.87(0.04)	19.54(0.02)	19.78(0.02)	20.01(0.03)	<i>J080213.44+242020.9</i>	20.23(0.04)	19.84(0.02)	20.00(0.02)	20.19(0.03)	25.85
CDDS14	J080644.09+444503.2	Y	18.54(0.02)	18.14(0.02)	18.32(0.01)	18.54(0.02)	J080643.64+444501.4	19.18(0.02)	18.74(0.02)	18.82(0.01)	18.94(0.02)	5.09
CDDS15	J084952.87+471249.4	Y	16.64(0.02)	16.77(0.02)	17.08(0.02)	17.35(0.02)	J084952.47+471247.7	18.14(0.14)	17.77(0.08)	17.79(0.06)	18.04(0.07)	4.37
CDDS16	J085915.02+330644.6	Y	18.27(0.02)	18.01(0.02)	18.34(0.02)	18.59(0.02)	J085915.50+330637.6	19.07(0.03)	18.70(0.02)	18.87(0.02)	19.04(0.02)	9.29
CDDS17	J085917.36+425031.6	Y	19.37(0.03)	18.94(0.05)	19.01(0.02)	19.08(0.02)	J085917.23+425027.4	18.83(0.02)	18.38(0.04)	18.53(0.02)	18.70(0.02)	4.39
CDDS18*	J092513.18+160145.4	L	17.07(0.09)	17.12(0.08)	17.52(0.06)	17.83(0.06)	J092513.48+160144.1	16.07(0.02)	16.14(0.02)	16.55(0.01)	16.88(0.02)	4.51
CDDS19 ^{D1}	J092647.00+132138.4	Y	18.74(0.03)	18.40(0.03)	18.46(0.05)	18.60(0.04)	J092646.88+132134.5	18.46(0.02)	18.34(0.02)	18.39(0.02)	18.50(0.02)	4.35
CDDS20	J095458.73+390104.6		20.31(0.05)	19.86(0.02)	19.95(0.03)	19.95(0.03)	<i>J095459.97+390052.4</i>	17.96(0.02)	17.69(0.02)	18.02(0.02)	18.29(0.02)	18.87
CDDS21	J100245.86+360653.3		19.42(0.03)	19.04(0.02)	19.09(0.02)	19.16(0.03)	<i>J100244.88+360629.6</i>	19.32(0.03)	18.92(0.02)	19.01(0.02)	19.09(0.03)	26.53
CDDS22 ^{D3}	J105306.13+025052.5	Y	19.57(0.04)	19.14(0.02)	19.28(0.02)	19.51(0.03)	<i>J105306.82+025027.9</i>	19.37(0.03)	18.98(0.02)	19.18(0.02)	19.37(0.03)	26.60
CDDS23	J113928.52-001420.9		19.84(0.04)	19.42(0.02)	19.52(0.02)	19.71(0.03)	J113928.47-001418.0	20.13(0.07)	19.80(0.06)	19.85(0.06)	19.93(0.08)	2.95
CDDS24	J115030.12+253210.1		20.43(0.05)	19.95(0.02)	19.97(0.02)	20.05(0.04)	J115030.48+253206.0	19.30(0.03)	18.86(0.02)	19.09(0.02)	19.29(0.02)	6.38
CDDS25	<i>J115305.54+005646.1</i>		18.42(0.02)	18.89(0.02)	19.38(0.02)	19.62(0.03)	J115305.47+005645.8	18.50(0.02)	18.91(0.02)	19.34(0.02)	19.78(0.03)	1.22
CDDS26 ^B	<i>J115937.81+134413.9</i>	Y	18.45(0.03)	18.07(0.02)	18.12(0.02)	18.16(0.02)	J115937.82+134408.7	18.42(0.03)	18.28(0.02)	18.52(0.02)	18.75(0.03)	5.18
CDDS27 ^{D3}	J122739.16+661224.4	Y	17.72(0.02)	17.86(0.02)	18.13(0.02)	18.44(0.02)	J122741.05+661224.3	18.23(0.02)	17.99(0.02)	18.21(0.02)	18.46(0.02)	11.43
CDDS28	<i>J131012.28+444728.3</i>		17.88(0.01)	17.84(0.02)	18.02(0.01)	18.23(0.02)	J131013.38+444717.8	17.95(0.01)	17.59(0.02)	17.85(0.01)	18.11(0.02)	15.71
CDDS29 ^B	J131332.14+203039.6	Y	18.13(0.02)	17.80(0.02)	17.98(0.01)	18.19(0.02)	J131332.56+203039.3	17.86(0.02)	17.48(0.02)	17.69(0.01)	17.91(0.02)	5.93
CDDS30	J131421.70+305051.4	Y	18.59(0.10)	18.20(0.08)	18.22(0.09)	18.31(0.09)	<i>J131421.50+305050.5</i>	18.23(0.04)	17.86(0.04)	17.88(0.05)	18.01(0.06)	2.76
CDDS31 ^B	J132814.28+163151.5	Y	16.34(0.02)	16.27(0.02)	16.63(0.02)	16.99(0.02)	J132814.36+163150.9	17.75(0.27)	17.65(0.23)	17.74(0.19)	17.84(0.15)	1.32
CDDS32	J135713.14-065913.7	Y	18.94(0.04)	19.25(0.02)	19.76(0.02)	20.18(0.04)	J135714.50-065856.9	18.58(0.04)	18.16(0.02)	18.35(0.02)	18.54(0.02)	26.29
CDDS33 ^{D1}	J150746.48+251002.1	Y	17.14(0.02)	16.91(0.03)	17.29(0.01)	17.55(0.02)	J150746.80+250958.0	17.98(0.02)	17.76(0.03)	18.06(0.01)	18.33(0.02)	5.05
CDDS34	J151508.30+143640.8	Y	18.38(0.02)	18.00(0.02)	18.20(0.01)	18.47(0.02)	J151507.90+143635.4	19.76(0.03)	19.63(0.02)	19.88(0.02)	20.19(0.03)	7.90
CDDS35	J154641.48+615901.7		19.07(0.03)	18.63(0.02)	18.75(0.02)	18.93(0.02)	J154641.79+615854.3	17.16(0.02)	16.89(0.02)	17.17(0.02)	17.42(0.02)	7.64
CDDS36	J155245.19+473129.5	Y	18.79(0.02)	18.71(0.02)	19.06(0.02)	19.36(0.03)	J155244.41+473124.0	19.21(0.04)	18.99(0.03)	19.30(0.02)	19.61(0.03)	9.65
CDDS37	J162650.11+482827.9		19.72(0.03)	19.62(0.02)	19.94(0.03)	20.20(0.04)	J162652.12+482824.7	19.14(0.02)	18.98(0.01)	19.30(0.02)	19.59(0.02)	20.22
CDDS38	J163647.81+092715.7		18.13(0.02)	17.72(0.01)	17.93(0.01)	18.18(0.01)	J163647.33+092708.4	19.98(0.04)	19.54(0.02)	19.54(0.02)	19.66(0.03)	10.12
CDDS39	<i>J165737.90+620102.1</i>		18.72(0.02)	18.65(0.01)	18.98(0.03)	19.23(0.02)	<i>J165734.39+620055.9</i>	18.88(0.02)	18.53(0.01)	18.76(0.02)	18.99(0.02)	25.47
CDDS40 ^B	<i>J170355.91+330438.4</i>	Y	19.16(0.02)	18.81(0.01)	18.86(0.01)	18.97(0.02)	<i>J170356.77+330435.7</i>	18.48(0.02)	18.16(0.01)	18.27(0.01)	18.42(0.02)	11.16
CDDS41	J173249.57+563900.0		19.35(0.03)	18.95(0.02)	19.12(0.02)	19.35(0.02)	J173249.32+563858.8	18.99(0.04)	19.12(0.05)	19.27(0.06)	19.47(0.04)	2.36
CDDS42	J175559.57+484359.9		19.04(0.03)	19.21(0.02)	19.39(0.02)	19.43(0.02)	J175558.35+484348.8	18.02(0.02)	17.68(0.01)	17.90(0.01)	18.17(0.02)	16.41
CDDS43	J204318.96+005841.8		18.51(0.03)	18.24(0.02)	18.42(0.01)	18.59(0.02)	J204317.93+005830.5	18.96(0.03)	18.59(0.02)	18.75(0.01)	18.94(0.02)	19.13
CDDS44	J211607.27+004503.1		18.60(0.02)	18.67(0.01)	18.89(0.01)	19.11(0.02)	J211607.20+004501.3	19.43(0.10)	18.96(0.07)	19.05(0.09)	19.28(0.06)	2.06
CDDS45	J213648.79+064320.2		18.07(0.02)	17.94(0.02)	18.24(0.01)	18.48(0.02)	J213648.98+064318.2	19.72(0.04)	19.35(0.02)	19.39(0.03)	19.50(0.02)	3.44
CDDS46	J214456.12+482352.9		19.19(0.03)	18.74(0.01)	18.83(0.02)	19.02(0.02)	J214457.39+482345.5	19.81(0.05)	19.49(0.02)	19.49(0.02)	19.64(0.03)	14.67
CDDS47	J215309.89+461902.7		18.15(0.02)	17.72(0.01)	17.90(0.01)	18.05(0.01)	J215308.90+461839.1	18.88(0.03)	19.08(0.01)	19.36(0.02)	19.56(0.02)	25.68
CDDS48 ^B	J22236.30-082808.0	Y	16.68(0.02)	16.41(0.02)	16.67(0.03)	16.92(0.03)	J22236.56-082806.0	17.56(0.03)	17.11(0.07)	17.30(0.07)	17.47(0.06)	4.29
CDDS49*	J222301.62+220131.3	L	15.66(0.01)	15.60(0.01)	15.91(0.01)	16.22(0.01)	J222301.72+220124.9	16.37(0.01)	16.01(0.03)	16.20(0.03)	16.46(0.01)	6.56
CDDS50 ^B	J22427.07+231537.4	Y	17.53(0.02)	17.15(0.02)	17.36(0.02)	17.47(0.02)	J22426.91+231536.0	18.22(0.08)	17.77(0.07)	17.92(0.07)	17.94(0.06)	2.64
CDDS51†	J224231.14+125004.9	L	16.48(0.01)	16.23(0.02)	16.50(0.01)	16.74(0.02)	J224230.33+125002.3	16.83(0.01)	16.50(0.02)	16.75(0.01)	16.97(0.02)	12.13
CDDS52 ^{D3}	J225932.74+140444.2	Y	19.02(0.03)	18.57(0.02)	18.68(0.01)	18.85(0.02)	J225932.21+140439.2	16.16(0.02)	16.36(0.01)	16.78(0.01)	17.12(0.01)	9.14
CDDS53	J233246.27+491712.0		18.76(0.02)	18.64(0.01)	18.91(0.01)	19.16(0.02)	<i>J233246.23+491709.1</i>	19.02(0.06)	18.76(0.04)	19.04(0.04)	19.31(0.05)	2.96

* PG 0922+162A+B (Finley & Koester 1997)

† HS 2220+2146A+B (Koester et al. 2009)

‡ HS 2240+1234 (Jordan et al. 1998)

^B Preliminary analysis presented in Baxter (2011)

^{D1, D2, D3} DA + DAH pairings discussed in (Dobbie et al. 2012a, 2013) and Dobbie et al. (in preparation), respectively.

3 SPECTROSCOPY

3.1 Observations and data reduction

While SDSS DR7 spectroscopy is available for objects in 18 of our systems (highlighted in italics in Table 1), it often covers only one of the sources in a pairing (e.g. CDDS 40; Kleinman et al. 2013), or, where the component angular separation is less than the diameter of the SDSS fibres (3 arcsec), it provides a blend of the energy distributions of the two objects (e.g. CDDS 11; Dobbie et al. 2013; Kepler et al. 2013). Therefore, to confirm or otherwise the degenerate nature of both components of the candidate binaries in Table 1 and to determine their fundamental parameters, we have acquired our own spatially resolved low-resolution optical spectroscopic observations with a range of facilities, as described below. As much of this spectroscopy was acquired in queue scheduling mode under less than optimum sky conditions, many of the systems we have followed up are from the brighter half of our sample and have angular separations that are greater than 2 arcsec. There is some minor overlap between our observations and the SDSS spectroscopy (CDDS 8-A + B, CDDS 26-B, CDDS 30-B and CDDS 40-A) and the results of the Kleinman et al. (2013) analyses of these DR7 data sets can serve as a useful check on our work.

For bona fide degenerate objects, we have used our new spectroscopic data to determine the dominant elemental component of their atmospheres and whether or not they harbour a substantial magnetic field. In this work, we have focused on the non-magnetic white dwarfs and have measured their effective temperatures and surface gravities by comparing suitable absorption features within their spectra (e.g. H-Balmer lines) to the predictions of modern model atmospheres. Spectroscopically observed pairings with at least one strongly magnetic component are analysed elsewhere (e.g. CDDS11, CDDS19, CDDS22, CDDS27, CDDS33, CDDS52; Dobbie et al. 2012a, 2013, Dobbie et al. in preparation). The five different telescopes we have sourced spectroscopy from are: the William Herschel Telescope (WHT) and the Gran Telescopio Canarias (GTC), both located at the Roche de las Muchachos Observatory on La Palma, Gemini-North at the Mauna Kea Observatory on Hawaii, Gemini-South at Cerro Pachon in Chile and the Very Large Telescope (VLT) Antu located at the European Southern Observatory's (ESO) Cerro Paranal site in Chile. Details of the observations obtained with each facility are provided below:

(i) Spectra of CDDS3, CDDS40 and CDDS50 were acquired in visitor mode with the WHT and the double-armed Intermediate Dispersion Spectrograph and Imaging System (ISIS) on the nights of 2008 July 24–25 and 2011 September 5. These observations were conducted when the sky was clear, with seeing ~ 0.6 – 0.9 arcsec. The spectrograph was configured with a 1.0 arcsec slit and the R300B ($\lambda/\delta\lambda \approx 1300$) grating on the blue arm. The long exposures necessary to reach good signal-to-noise ratio were broken down into several integrations of typically 1800 s (see Table 2), and were acquired using the 2×1 and 1×1 binning modes of the E2V CCD during the 2008 and 2011 runs, respectively. The data frames were debiased and flat fielded using the IRAF procedure CCDPROC. Cosmic ray hits were removed using the routine LACOS SPEC (van Dokkum 2001). Subsequently, the spectra were extracted with the APEXTRACT package and wavelength calibrated by comparison with a CuAr+CuNe arc spectrum taken immediately before and after the science exposures. The removal of remaining instrument signature from the science data was undertaken using observations of the bright DC white dwarfs WD 1918+386 and EG131.

(ii) Spectra of CDDS8, CDDS26, CDDS29, CDDS30, CDDS31 and CDDS32 were obtained in visitor mode with VLT Antu and the Focal Reducer and low dispersion Spectrograph (FOR2). A full description of the FOR2 instrument may be found on the ESO webpages.¹ These observations were conducted on the nights of 2010 February 6–7 and 2013 February 10–11. The sky conditions were fair to good at the time of these observations. All data were acquired using the 2×2 binning mode of the E2V CCD and the 600B+24 grism. A 1.3 arcsec wide and a 1.0 arcsec wide slit were used for the 2010 and 2013 observations, respectively, providing notional spectral resolutions of $\lambda/\delta\lambda \sim 600$ and $\lambda/\delta\lambda \sim 800$. The data were reduced and extracted with IRAF routines, as per the ISIS spectra, and wavelength calibrated by comparison with a He+HgCd arc spectrum obtained within a few hours of the science frames. Remaining instrument signature was removed from the science data using observations of the bright DC white dwarf LHS2333.

(iii) Spectra of CDDS6 and CDDS48 were obtained in service mode with the Gemini Multi-Object Spectrograph (GMOS) mounted on the Gemini-North and Gemini-South telescopes during semesters 2009B (July 25) and 2010A (May 11), respectively. These observations were conducted when the sky conditions were relatively poor (image quality 85 per cent and cloud cover 90 per cent). The data were acquired using the 4×4 binning mode of the EEV CCD, a 2.0 arcsec wide slit and the B600 grating tuned to a central wavelength of 4100 Å. The notional resolution of these spectra is $\lambda/\delta\lambda \sim 600$. The data were reduced and extracted using routines in the GEMINI IRAF software package. A wavelength solution for these data was obtained with a CuAr arc spectrum obtained within hours of the science frames, while residual instrument signature in the science data was removed using observations of the bright DC white dwarfs WD 1918+386 (north) and WD 0000-345 (south).

(iv) Spectra of CDDS9, CDDS14, CDDS15, CDDS16, CDDS17, CDDS34 and CDDS36 were acquired in service mode with the GTC and the Optical System for Imaging and low Resolution Integrated Spectroscopy (OSIRIS) during semester 2013A. A detailed description of the OSIRIS instrument is provided on the GTC webpages.² Our observations were performed when sky conditions were less favourable (seeing ≈ 1.2 – 1.5 arcsec and spectroscopic transparency), using the 2×2 binning mode of the EEV CCD. With the R1000B grating, in conjunction with a 1.2 arcsec wide slit, we achieved a notional spectral resolution of $\lambda/\delta\lambda \approx 500$. The data were reduced and extracted with IRAF routines as per the ISIS spectra. Wavelength calibration was performed by comparing these to a Hg + Ne arc spectrum acquired within a few hours of the science frames. Particular care was taken to include the 3650.1 Å Hg I line at the very blue limit of our spectral coverage in our arc wavelength solution. Remaining instrument signature from the science data was removed using observations of the bright DC white dwarf WD 1918+386.

The spectroscopic observations are summarized in Table 2. We noted above that three of our CDDS have been the subjects of previous spectroscopic studies, PG 0922+162 (Finley & Koester 1997), HS 2220+2146 (Koester et al. 2009) and HS 2240+1234 (Jordan et al. 1998). Throughout the rest of this work we adopt the parameters measured from a high-spectral resolution Koester et al. (2009) investigation of the components of these three pairings. We

¹ <http://www.eso.org/instruments/fors2/>

² <http://www.gtc.iac.es/instruments/osiris/osiris.php>

Table 2. Summary of our spectroscopic observations, including telescope/instrument combination and exposure times, of the candidate young, wide, double-degenerates within the SDSS DR7 imaging (RA = 0–12h).

ID	SpT	SDSS	Telescope/Instrument	Exposure	N_{exp}
CDDS3-A	DA	J005212.73+135301.1	WHT + ISIS	2400 s	5
CDDS3-B	DA	J005212.26+135302.0			
CDDS6-A	DA	J021131.52+171428.3	GEM-N + GMOS	2000 s	3
CDDS6-B	DA	J021131.51+171430.4			
CDDS8-A	DA	J033236.86-004936.9	VLT + FORS	600 s	2
CDDS8-B	DA	J033236.60-004918.4			
CDDS9-A	DA	J054519.81+302754.0	GTC + OSIRIS	2400 s	3
CDDS9-B	DA	J054518.98+302749.3			
CDDS14-A	DA	J080644.09+444503.2	GTC + OSIRIS	600 s	3 ^{>}
CDDS14-B	DA	J080643.64+444501.4			
CDDS15-A	DB	J084952.87+471249.4	GTC + OSIRIS	240 s	3
CDDS15-B	DA	J084952.47+471247.7			
CDDS16-A	DA	J085915.50+330637.6	GTC + OSIRIS	600 s	3
CDDS16-B	DA	J085915.02+330644.6			
CDDS17-A	DA	J085917.36+425031.6	GTC + OSIRIS	900 s	3
CDDS17-B	DA	J085917.23+425027.4			
CDDS18-A*	DA	J092513.48+160144.1	Koester et al. (2009)		
CDDS18-B*	DA	J092513.18+160145.4			
CDDS26-A	DA	J115937.82+134408.7	VLT + FORS	600 s	2
CDDS26-B	DA	J115937.81+134413.9			
CDDS29-A	DA	J131332.56+203039.3	VLT + FORS	300 s	2
CDDS29-B	DA	J131332.14+203039.6			
CDDS30-A	DA	J131421.70+305051.4	VLT + FORS	600 s	2
CDDS30-B	DA	J131421.50+305050.5			
CDDS31-A	DA	J132814.36+163150.9	VLT + FORS	300 s	2
CDDS31-B	DA	J132814.28+163151.5			
CDDS32-A	DA	J135714.50-065856.9	VLT + FORS	600 s	1
CDDS32-B	sdO	J135713.14-065913.7			
CDDS34-A	DA	J151508.30+143640.8	GTC + OSIRIS	1800 s	3
CDDS34-B	DA	J151507.90+143635.4			
CDDS36-A	DA	J155245.19+473129.5	GTC + OSIRIS	900 s	3
CDDS36-B	DA	J155244.41+473124.0			
CDDS40-A	DA	J170356.77+330435.7	WHT + ISIS	1800 s	7
CDDS40-B	DA	J170355.91+330438.4			
CDDS48-A	DA	J222236.56-082806.0	GEM-S + GMOS	1800 s	3
CDDS48-B	DA	J222236.30-082808.0			
CDDS49-A ⁺	DA	J222301.72+220124.9	Koester et al. (2009)		
CDDS49-B ⁺	DA	J222301.62+220131.3			
CDDS50-A	DA	J222427.07+231537.4	WHT + ISIS	1200 s	2
CDDS50-B	DA	J222426.91+231536.0			
CDDS51-A [†]	DA	J224231.14+125004.9	Koester et al. (2009)		
CDDS51-B [†]	DA	J224230.33+125002.3			

* PG 0922+162A+B (Finley & Koester 1997).

⁺ HS 2220+2146A+B (Koester et al. 2009)[†] HS 2240+1234 (Jordan et al. 1998)

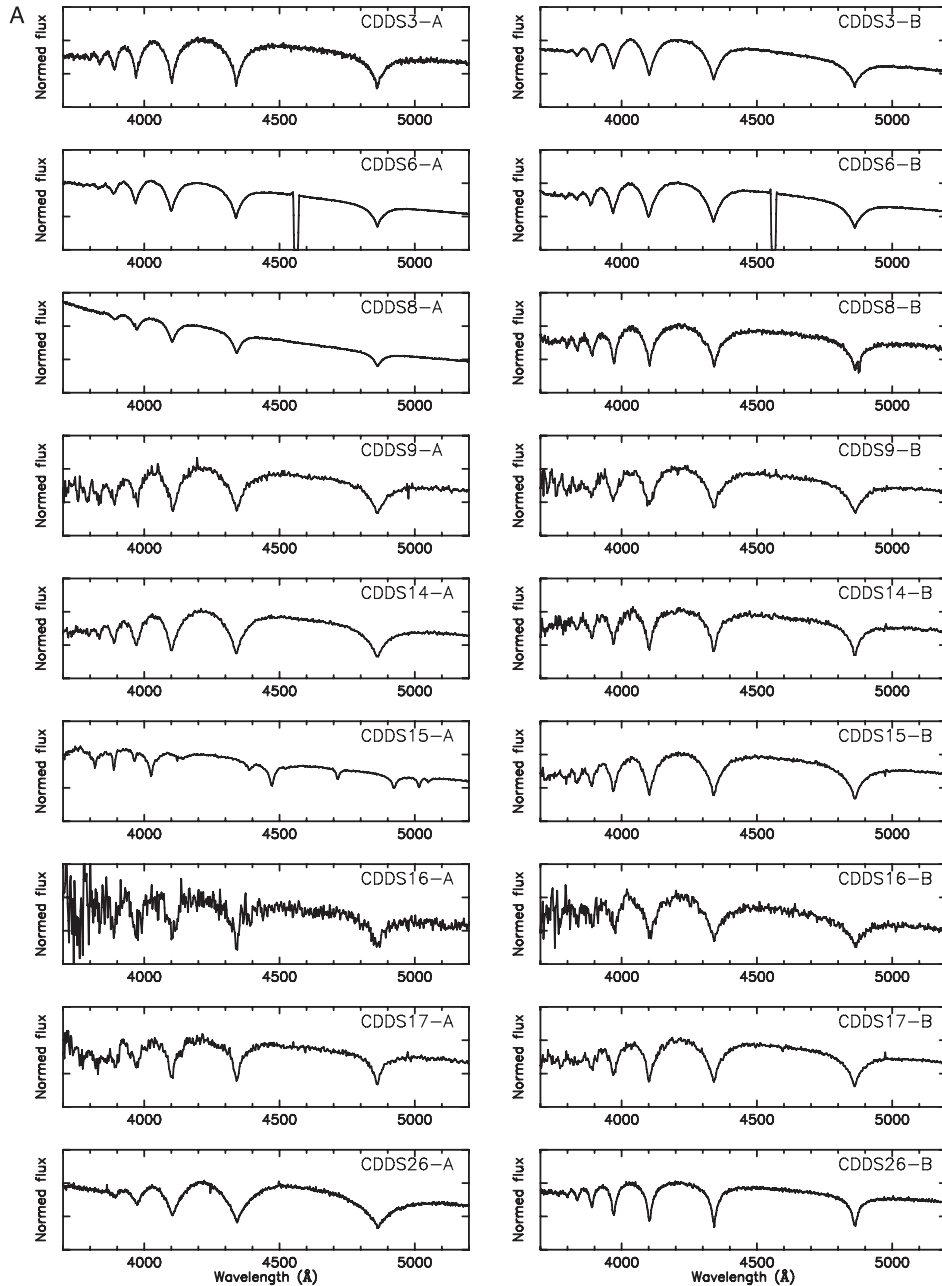


Figure 2. Low-resolution optical spectroscopy for the components of candidate binary systems in the range (a) RA = 0–12 h and (b) RA = 12–24 h. These data have been normalized by dividing by the median flux in the interval $\lambda = 4180\text{--}4220 \text{ \AA}$.

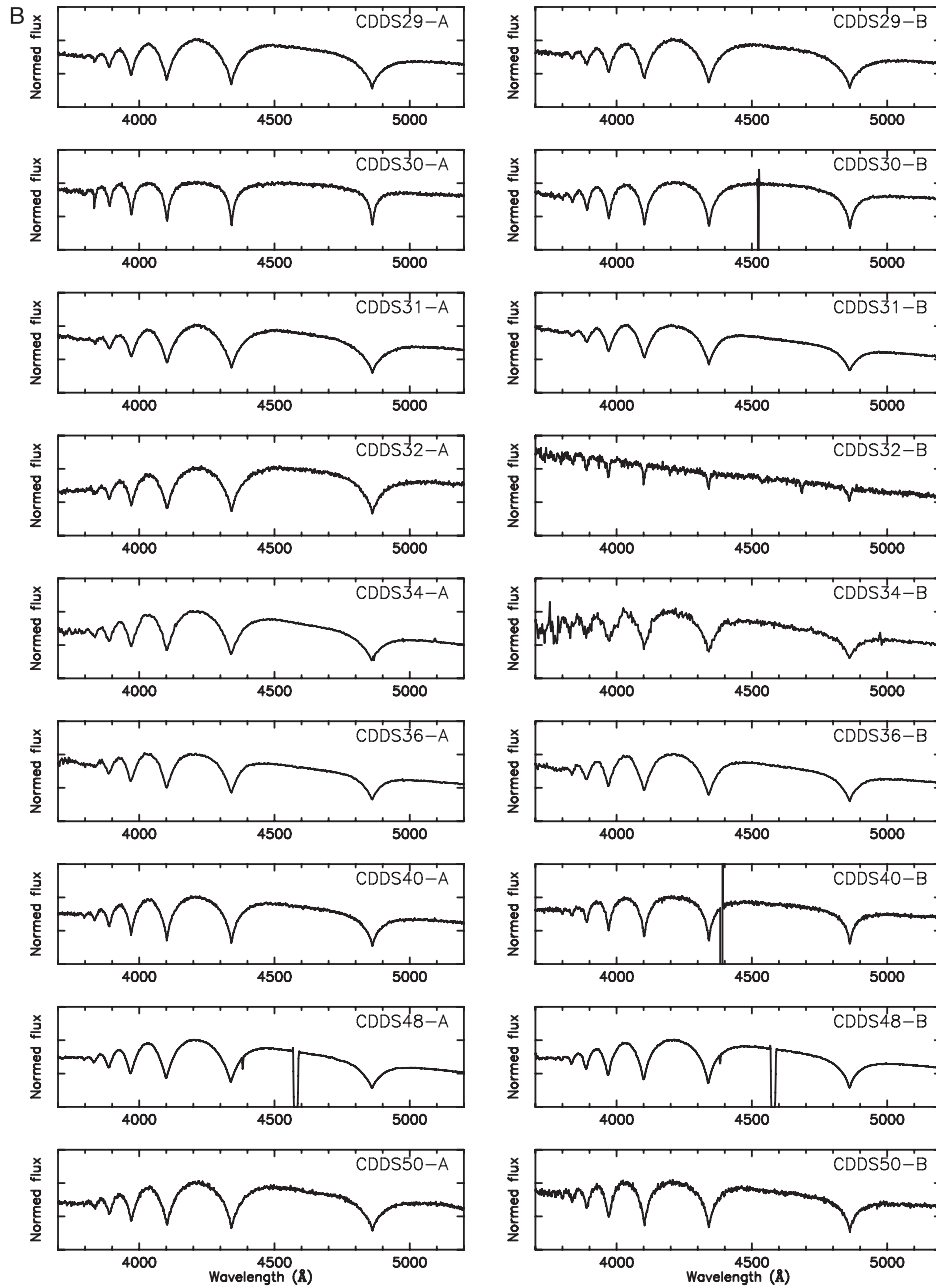
re-affirm their results for HS 2220+2146 from our measurements of a low-resolution Gemini-N/GMOS spectrum ($T_{\text{eff}} = 19\,020 \pm 438$, $\log g = 8.37 \pm 0.07$ and $T_{\text{eff}} = 13\,950 \pm 321$, $\log g = 8.07 \pm 0.07$ for SDSS J222301.62+220131.3 and SDSS J222301.72+220124.9, respectively).

4 DATA ANALYSIS

4.1 White dwarfs, effective temperatures, surface gravities and distances

Our optical spectroscopy (Fig. 2) reveals through the presence of broad H-Balmer line series, that the overwhelming majority of the

objects we have followed up are white dwarfs with hydrogen-rich atmospheres (DAs). As discussed in companion papers, all the non-magnetic white dwarfs in six additional spectroscopically observed pairings harbouring a strongly magnetic component, also appear to have hydrogen-dominated atmospheres (e.g. Dobbie et al. 2012a, 2013). The spectrum of one object in our sample, CDDS15-A (SDSS J084952.87+471249.4), features strong, pressure broadened, He I lines, consistent with it being a degenerate with a helium-dominated atmosphere (DB). The energy distribution of CDDS32-B (SDSS J135713.14–065913.7) appears to be that of an evolved subdwarf star (sdO) which is likely to be located at a distance of several kiloparsec (compared to only several hundred parsec for the white dwarf CDDS32-A). Consequently, the CDDS32 pairing is not considered further.

Figure 2 – *continued*

We have measured the effective temperatures and surface gravities of the DAs by comparing the observed lines, H- δ to H- β , to a grid of synthetic profiles based on recent versions of the plane-parallel, hydrostatic, local thermodynamic equilibrium atmosphere and spectral synthesis codes `ATM` and `SYN` (e.g. Koester 2010). These models include an updated physical treatment of Stark broadening of H I lines (Tremblay & Bergeron 2009). The effective temperature and surface gravity of the DB (CDDS15-A) has been measured by comparing the normalized observed energy distribution within the wavelength range 3750–5150 Å, to a grid of similarly normalized synthetic spectra. These were also generated using `ATM` and `SYN`, in this case tuned for the treatment of helium rich atmospheres. Our model fitting was undertaken with the spectral analysis package

`XSPEC` (Shafer 1991) as described in previous work (e.g. Dobbie et al. 2009). The errors in our parameters determinations have been calculated by stepping that in question away from its optimum value until the difference between the two values of the fit statistic ($\Delta\chi^2$), corresponds to 1σ for a given number of free model parameters (e.g. Lampton, Margon & Bowyer 1976). However, as these are only formal (internal) estimates of the errors on effective temperature and surface gravity, and may underestimate the true uncertainties, we have assumed their magnitudes to be at least 2.3 per cent and 0.07 dex, respectively, for the DA stars (Napiwotzki, Green & Saffer 1999) and at least 2.3 per cent and 0.05 dex, respectively, for the DB-type objects (Bergeron et al. 2011). In cases where the fitting provided two solutions for the effective

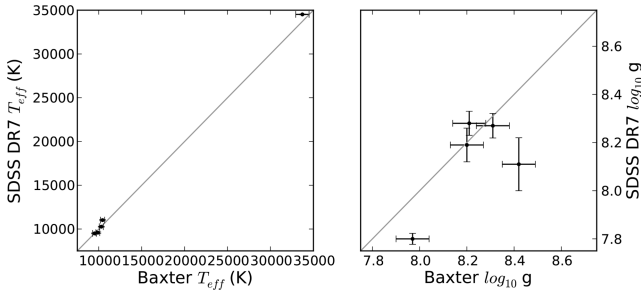


Figure 3. Plot of our estimates of effective temperature and surface gravity against the SDSS DR7 spectroscopic-based measurements of Kleinman et al. (2013) for five white dwarfs in common to our spectroscopic sample and the DR7 white dwarf catalogue.

temperature of a star, we compared its observed photometry to synthetic colours (e.g. Bergeron, Wesemael & Beauchamp 1995) to break the degeneracy.

The results of our analysis procedure are listed in Table 3. As can be seen from Fig. 3, our measurements of these parameters for the five objects that are common to both the DR7 white dwarf catalogue and our spectroscopic follow-up are generally accordant with those of Kleinman et al. (2013). The surface gravity estimates for CDDS 8-A and CDDS 40-B deviate at around 2σ from the one-to-one relation. It is conceivable that these differences are statistical in nature but, considering our observations for both these objects have provided data of excellent signal-to-noise ratio for the gravity sensitive spectral features, systematic error could also be the cause. The former object is the hottest white dwarf in our spectroscopic sample and has relatively weak high order Balmer lines in the wavelength regime ($\lambda < 4000 \text{ \AA}$) where the response of the SDSS spectrographs changes shape (decreases) rapidly. The effective temperature we measure for CDDS 8-B is also lower by around 500 K than the Kleinman et al. (2013) determination, yet both the SDSS data and our spectrum for this object provide strong signal-to-noise coverage of the potent temperature diagnostic Balmer lines e.g. $H\gamma$ and $H\beta$. We discuss this object in more detail in Section 7.3, but for now note that it is a pulsating white dwarf.

Subsequently, we have derived the absolute r magnitudes of each white dwarf by interpolating (using cubic-splines) within grids of modern synthetic photometry³ to the measured effective temperature and surface gravity. The He-rich grids, relevant to CDDS15-A, originate from the work of Bergeron et al. (2011). The H-rich grids, appropriate to the DAs, are based on the work of Bergeron et al. (1995) but revised to include updates from Holberg & Bergeron (2006), Kowalski & Saumon (2006) and Tremblay et al. (2011). Spectroscopically derived effective temperatures and surface gravities are known to lead to systematic overestimates of DA white dwarf masses at $T_{\text{eff}} < 12\,500 \text{ K}$ (e.g. Bergeron et al. 1995; Kepler et al. 2007). We have adjusted the derived parameters of our affected objects by subtracting mass offsets, which have been determined from the data points shown in fig. 19 of Tremblay et al. (2011). These data points have been verified to provide a fair representation of the systematic overestimate through examining them with respect to the departures between the two mass estimates we have made for the subset of our cool degenerates that are paired with a white dwarf with $T_{\text{eff}} > 12\,500 \text{ K}$, i.e. the wholly spectroscopic mass estimate and the mass derived from the spectroscopic

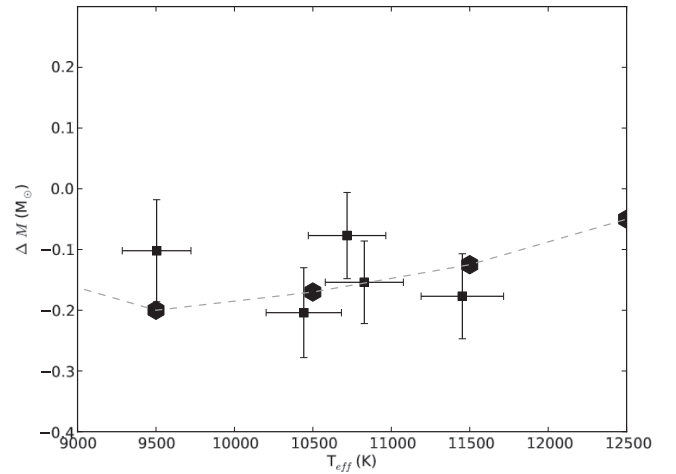


Figure 4. Plot of the departures between the wholly spectroscopically derived mass and that derived from the spectroscopic effective temperature and the SDSS photometry under the assumption that the components lie at the same distance, for five white dwarfs with $T_{\text{eff}} < 12\,500 \text{ K}$ in wide double-degenerate pairings where the companion stars have $T_{\text{eff}} > 12\,500 \text{ K}$ and the components have highly significant and consistent proper motions (filled squares, from left to right, CDDS26-B, CDDS8-B, CDDS50-B, CDDS3-A and CDDS48-A). The increase in the mean spectroscopic mass below $T_{\text{eff}} < 12\,500 \text{ K}$, with respect to the value at $T_{\text{eff}} > 13\,000 \text{ K}$, found by Tremblay, Bergeron & Gianninas (2011) in their study of the SDSS DR4 white dwarf sample is also shown (filled hexagons and dashed line).

effective temperature and the SDSS photometry under the assumption that the components lie at the same distance (Fig. 4 and next section). Finally, to help appraise the physical reality of our pairs we have calculated the distance moduli of the white dwarfs, neglecting foreground extinction (Table 3 and Fig. 5). Dust maps suggest that this is very low along the majority of these Galactic lines of sight (Schlegel, Finkbeiner & Davis 1998). Moreover, our conclusions are primarily sensitive to differential reddening and given the angular proximity of our targets, for physical systems this is likely to be very small.

4.2 Astrometry

To assess further the physical reality of our candidate binaries, we have performed astrometry on their components. In the majority of cases, we have conducted these measurements with the positions of sources from the full United States Naval Observatory B1.0 (USNO-B) catalogue (Monet et al. 2003) and from the SDSS. We have followed a methodology similar to that adopted by Kraus & Hillenbrand (2007) and the PPMXL survey (Roeser, Demleitner & Schilbach 2010) to shift the former on to the International Celestial Reference System (ICRS). In brief, we determined the tangent plane coordinates, ξ and η , corresponding to each photographic epoch, for all sources within several degrees of our pairs from their catalogued year 2000.0 positions, their tangent plane proper motions, their fit residuals and the dates of their photographic imaging. We next calculated for each object the celestial coordinates at the mean USNO epoch and at all photographic epochs (J2000.0) with the catalogued positions, the tangent plane coordinates for epoch 2000.0 and routines in STARLINK SLALIB. Subsequently, we cross-correlated sources brighter than $R2 = 16.5 \text{ mag.}$ with objects listed in the Fourth United States Naval Observatory CCD Astrograph Catalog (UCAC4; Zacharias et al. 2013) that have low proper motions ($\mu < 5 \text{ mas yr}^{-1}$) and small proper motion

³ <http://www.astro.umontreal.ca/bergeron/CoolingModels>

Table 3. Our effective temperature and surface gravity measurements for the components of the wide white dwarf + white dwarf candidate binary systems. The predicted absolute r magnitudes, distance moduli, masses and proper motions for these objects are also listed. Where deemed necessary, parameters have been modified to account for the spectroscopic overestimate of mass which occurs at $T_{\text{eff}} < 12\,500$ K (column 4; see text for further details). An assessment of the physical nature of each pairing has been made by considering a Bayes factor estimated from the distances and the astrometry of the components.

ID	T_{eff} (K)	$\log g$ ($\log_{10}(\text{cm s}^{-2})$)	ΔM (M_{\odot})	M_r (mag)	$r - M_r$ (mag)	M (M_{\odot})	$\mu_{\alpha} \cos \delta, \mu_{\delta}$ (mas yr^{-1})	$\frac{P(\text{data} C)}{P(\text{data} F)}$	DD?
CDDS3-A	10 828 ± 249	8.16 ± 0.07	−0.16	11.87 ^{+0.16} _{−0.16}	7.05 ± 0.17	0.54 ± 0.06	4.7 ± 4.4, −41.6 ± 4.4	345	✓
CDDS3-B	19 116 ± 440	7.94 ± 0.07	−	10.96 ^{+0.12} _{−0.12}	7.02 ± 0.11	0.59 ± 0.04	8.6 ± 4.4, −41.8 ± 4.4		
CDDS6-A	24 788 ± 570	8.06 ± 0.07	−	10.69 ^{+0.11} _{−0.12}	6.39 ± 0.12	0.67 ± 0.04	−50.9 ± 18.3, −2.6 ± 10.7	91	✓
CDDS6-B	18 502 ± 426	8.06 ± 0.07	−	11.19 ^{+0.11} _{−0.11}	6.46 ± 0.14	0.65 ± 0.04	−34.7 ± 18.3, 3.6 ± 10.7		
CDDS8-A	33 725 ± 776	7.97 ± 0.07	−	9.90 ^{+0.13} _{−0.12}	6.19 ± 0.13	0.64 ± 0.04	−31.2 ± 3.2, −23.6 ± 3.2	1395	✓
CDDS8-B	10 442 ± 240	8.31 ± 0.07	−0.17	12.18 ^{+0.17} _{−0.16}	6.12 ± 0.17	0.63 ± 0.06	−28.4 ± 3.2, −23.9 ± 3.2		
CDDS9-A	11 636 ± 410	7.95 ± 0.13	−0.11	11.51 ^{+0.24} _{−0.25}	8.45 ± 0.25	0.47 ± 0.04	−4.0 ± 3.9, −9.8 ± 3.9	11	✓
CDDS9-B	16 410 ± 524	7.96 ± 0.11	−	11.25 ^{+0.17} _{−0.17}	8.55 ± 0.17	0.59 ± 0.05	2.6 ± 4.1, −14.2 ± 3.9		
CDDS14-A	12 185 ± 280	8.11 ± 0.07	−0.07	11.76 ^{+0.15} _{−0.14}	6.56 ± 0.15	0.60 ± 0.06	4.0 ± 3.2, −2.1 ± 3.2	130	✓
CDDS14-B	10 140 ± 233	8.23 ± 0.08	−0.18	12.12 ^{+0.18} _{−0.18}	6.70 ± 0.18	0.56 ± 0.06	5.6 ± 3.2, −0.4 ± 3.2		
CDDS15-A	16 992 ± 391	7.84 ± 0.07	−	10.92 ^{+0.11} _{−0.11}	6.16 ± 0.12	0.51 ± 0.04	−88.0 ± 3.0, −76.9 ± 3.0	>10000	✓
CDDS15-B	11 127 ± 256	8.08 ± 0.07	−0.14	11.72 ^{+0.16} _{−0.16}	6.07 ± 0.17	0.51 ± 0.06	−82.3 ± 3.0, −76.5 ± 3.0		
CDDS16-A	11 032 ± 872	7.94 ± 0.39	−0.15	11.48 ^{+0.70} _{−0.90}	7.39 ± 0.81	0.42 ± 0.22	3.0 ± 4.1, 3.4 ± 4.1	10	✓
CDDS16-B	11 837 ± 824	8.21 ± 0.18	−0.10	11.89 ^{+0.35} _{−0.40}	6.45 ± 0.35	0.63 ± 0.12	−0.8 ± 4.1, −0.3 ± 4.1		
CDDS17-A	10 074 ± 232	8.46 ± 0.13	−0.18	12.51 ^{+0.25} _{−0.24}	6.50 ± 0.25	0.71 ± 0.09	15.3 ± 2.9, −15.1 ± 2.9	119	✓
CDDS17-B	11 083 ± 254	8.23 ± 0.08	−0.15	11.95 ^{+0.17} _{−0.17}	6.58 ± 0.18	0.60 ± 0.06	14.3 ± 2.9, −9.2 ± 2.9		
CDDS26-A	16 401 ± 377	8.94 ± 0.07	−	12.93 ^{+0.15} _{−0.14}	5.59 ± 0.15	1.17 ± 0.03	−19.9 ± 3.0, −42.8 ± 3.0	1266	✓
CDDS26-B	9504 ± 219	8.20 ± 0.07	−0.20	12.24 ^{+0.18} _{−0.18}	5.88 ± 0.18	0.52 ± 0.06	−21.1 ± 3.0, −45.2 ± 3.0		
CDDS29-A	12 758 ± 293	8.18 ± 0.07	−	11.96 ^{+0.11} _{−0.10}	5.73 ± 0.11	0.72 ± 0.04	−31.6 ± 2.9, 26.4 ± 2.9	1992	✓
CDDS29-B	13 072 ± 301	8.41 ± 0.07	−	12.28 ^{+0.12} _{−0.11}	5.70 ± 0.12	0.87 ± 0.05	−26.8 ± 2.9, 27.8 ± 2.9		
CDDS30-A*	9203 ± 212	8.14 ± 0.07	−0.18	12.30 ^{+0.17} _{−0.18}	5.92 ± 0.20	0.50 ± 0.06	−45.3 ± 14.9, 33.5 ± 14.8	125	✓
CDDS30-B	10 293 ± 237	8.21 ± 0.07	−0.18	12.04 ^{+0.17} _{−0.18}	5.84 ± 0.18	0.55 ± 0.06	−43.1 ± 14.9, 32.5 ± 14.8		
CDDS31-A	14 037 ± 323	8.45 ± 0.07	−	12.25 ^{+0.12} _{−0.12}	5.49 ± 0.22	0.89 ± 0.05	−26.3 ± 27.3, 20.0 ± 12.7	54	✓
CDDS31-B	20 000 ± 460	8.19 ± 0.07	−	11.27 ^{+0.12} _{−0.12}	5.36 ± 0.12	0.74 ± 0.04	−50.8 ± 27.3, 22.8 ± 12.7		
CDDS34-A	14 100 ± 398	7.86 ± 0.07	−	11.37 ^{+0.11} _{−0.11}	6.83 ± 0.11	0.53 ± 0.04	0.2 ± 3.5, −22.2 ± 3.5	≪1	×
CDDS34-B	18 261 ± 598	7.90 ± 0.12	−	10.98 ^{+0.18} _{−0.18}	9.00 ± 0.19	0.56 ± 0.07	0.1 ± 3.5, −0.2 ± 3.5		
CDDS36-A	18 769 ± 432	7.94 ± 0.07	−	10.99 ^{+0.11} _{−0.11}	8.06 ± 0.11	0.59 ± 0.04	−5.7 ± 4.2, −12.5 ± 4.2	72	✓
CDDS36-B	16 542 ± 380	7.91 ± 0.07	−	11.16 ^{+0.11} _{−0.11}	8.14 ± 0.11	0.57 ± 0.04	−7.7 ± 4.2, −7.7 ± 4.2		
CDDS40-A	11 207 ± 258	8.22 ± 0.07	−0.14	11.93 ^{+0.16} _{−0.16}	6.34 ± 0.16	0.60 ± 0.06	2.5 ± 3.1, −50.8 ± 3.1	2418	✓
CDDS40-B	9888 ± 227	8.42 ± 0.07	−0.19	12.48 ^{+0.17} _{−0.16}	6.38 ± 0.17	0.68 ± 0.06	1.3 ± 3.1, −50.6 ± 3.1		
CDDS48-A	11 453 ± 263	8.35 ± 0.07	−0.13	12.11 ^{+0.16} _{−0.15}	5.19 ± 0.17	0.69 ± 0.06	−2.3 ± 8.4, −29.2 ± 7.4	2530	✓
CDDS48-B	15 834 ± 364	8.02 ± 0.07	−	11.40 ^{+0.11} _{−0.11}	5.27 ± 0.11	0.63 ± 0.04	−0.0 ± 8.4, −28.0 ± 7.4		
CDDS50-A	12 739 ± 293	8.04 ± 0.07	−	11.76 ^{+0.10} _{−0.10}	5.60 ± 0.11	0.63 ± 0.04	38.3 ± 10.8, −0.9 ± 8.8	126	✓
CDDS50-B	10 718 ± 247	8.26 ± 0.07	−0.16	12.06 ^{+0.16} _{−0.16}	5.86 ± 0.18	0.60 ± 0.06	32.8 ± 10.8, −0.9 ± 8.8		

†Proper motion measurements are obtained with respect to nearby stars.

*Possible triple system, dK + WD + WD.

uncertainties ($\Delta\mu < 5$ mas yr^{−1}). We derived the ICRS positions of the matched objects at each photographic epoch and finally, estimated any offsets between these and the USNO-B coordinates using a maximum-likelihood technique.

We calculated absolute proper motions by performing a least-squares linear fit in each axis to the USNO-B coordinates on the ICRS and the SDSS positions as a function of date, weighting according to crude uncertainty estimates of 50 and 230 mas for SDSS

and photographic epochs, respectively (e.g. Kraus & Hillenbrand 2007; Roeser et al. 2010). In this final step, we used only astrometry from photographic images where a visual inspection revealed the components to be clearly resolved. In cases where there was mild blending we relied on SExtractor (Bertin & Arnouts 1996) and a Mexican hat filter for a more robust discrimination of the components and their photocentres. However, several of our pairings were found to be sufficiently blended in all photographic epochs that we

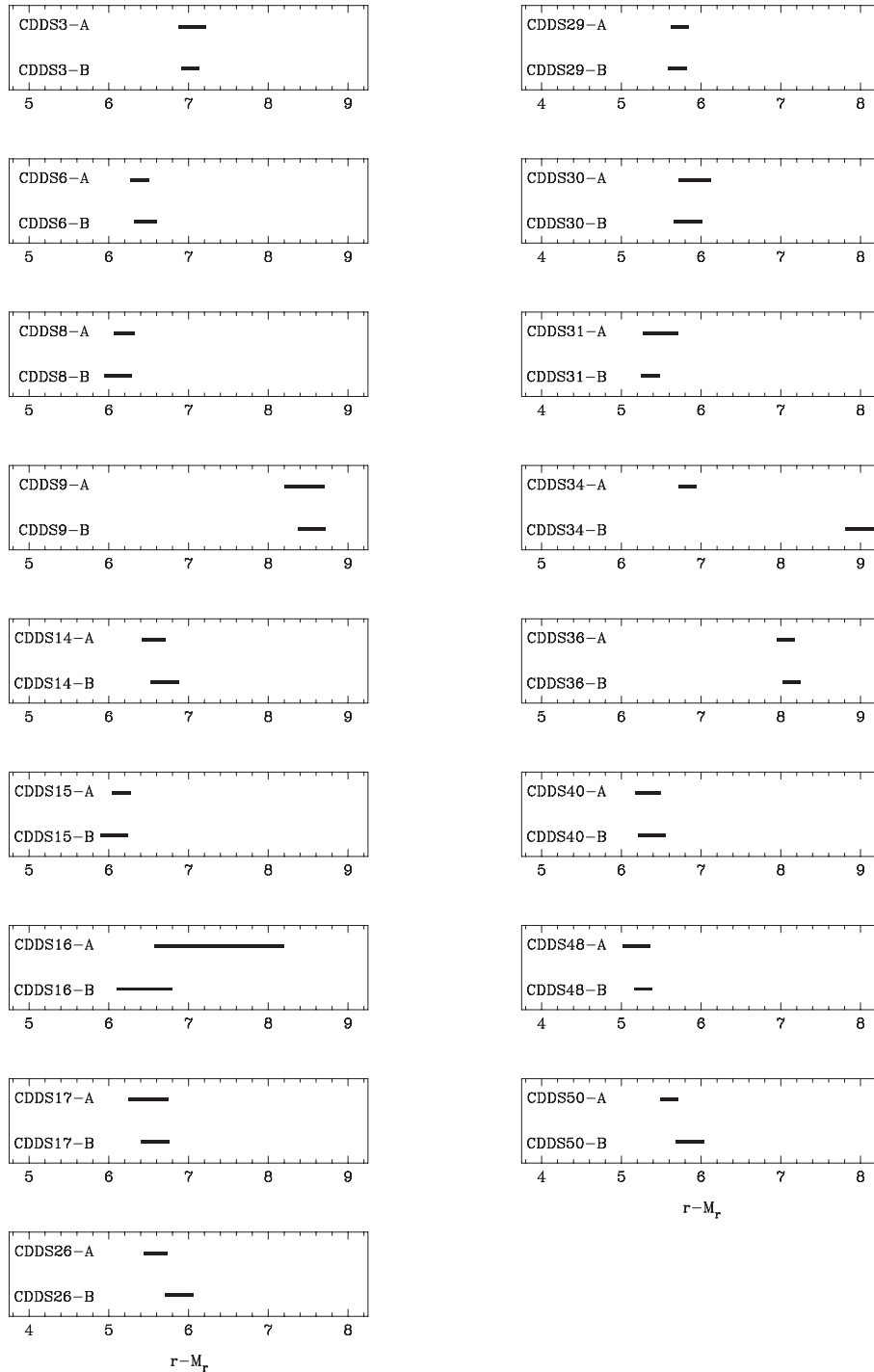


Figure 5. The derived distance moduli of the white dwarfs in our candidate binaries. The components of all but one system have consistent distances, as expected for physical binary systems.

had to adopt a different approach. In these cases we generally relied on the SDSS DR7 r -band coordinates as a first epoch and positions from additional electronic imaging for the second epoch. We obtained i -band frames for CDDS6A and CDDS31 on 2011 February 12 using the Isaac Newton Telescope and Wide Field Camera. We extracted positions from J -band United Kingdom Infrared telescope Deep Sky Survey (UKIDSS; Hewett et al. 2006; Casali et al. 2007; Lawrence et al. 2007; Hambly et al. 2008; Hodgkin et al. 2009; 2010 February 22) and Y -band Visible and Infrared Survey

Telescope for Astronomy (VISTA; McMahon 2012; 2012 September 9) imaging for CDDS30 and CDDS48, respectively. Positions for the components of CDDS50 were obtained from two epochs of SDSS r -band imaging separated by approximately 5 yr (2004 September 17 and 2009 October 17). We employed routines in the STARLINK SLALIB library to construct six coefficient linear transforms between the two sets of coordinates for each putative system, iteratively clipping 3σ outliers from the fits (e.g. Dobbie et al. 2002). Subsequently, we determined relative proper motions by taking the

differences between the observed and calculated locations of candidates in the second epoch imaging and dividing by the time baseline between the two observations. Astrometric measurements for the components of all spectroscopically observed pairs are displayed in Table 3.

4.3 Physical system or chance alignment?

A casual inspection of Fig. 5 reveals that our distance moduli estimates for the components in most pairings overlap with one and other. Moreover, the white dwarfs in 10 out of the 17 new candidate binaries have proper motions that are both significant ($\mu/\delta\mu \gtrsim 3$) and internally consistent, supporting the notion that a sizeable majority of our pairs are physical systems. Only one system, CDDS 34, displays a large and statistically significant (greater than 5σ) disparity between the distance moduli of its components. Our astrometric measurements also appear strongly discordant (by 4σ on the declination axis) for the components of this system. While we could simply dismiss this one candidate out of hand and accept the others as bona fide binary systems, we have attempted to assess the physical reality of all 17 pairs more quantitatively within a ‘Naive’ Bayesian scheme (e.g. Zheng 1998).

In this approach, we adopted the brightest object (at r) in each pair as a putative primary star and estimated a Bayes factor for two competing models that can account for the secondary component. We assumed that it could be either a physical companion (C) or a field white dwarf (F) such that the sum of the probabilities, $P(C)$, it is a companion and $P(F)$, it is a field star, $P(C) + P(F) = 1$. Considering each candidate binary in turn, we first defined a probability distribution function for the distance of the secondary star, in case it is a field white dwarf, $P(\text{dist} | F)$. We divided the visibility cone in the direction of the pair into a series of thin slices (out to 1250 pc) and integrated the luminosity function of De Gennaro et al. (2008) over the bolometric magnitude range that is consistent with our survey limits and the mean distance of each slice (adopting $\log g = 8.0$ white dwarfs and using the synthetic photometry of the Montreal group to translate between M_{bol} and M_r) to obtain estimates of the number of white dwarfs per cubic parsec. After factoring in the 300 pc Galactic scaleheight of the white dwarf population (e.g. Vennes et al. 2002), we multiplied the resulting values by the slice volumes to obtain the number of objects within each region along the visibility cone. This distribution function was normalized over the range 0–1250 pc, outwith of which it is effectively zero (due to the magnitude limit of our survey).

Next, we defined a probability distribution function for the proper motion of the secondary star in case it is a field white dwarf, $P(\text{pm} | F)$. We obtained absolute proper motions from the SuperCOSMOS Sky Survey data base (Hambly et al. 2001) for all white dwarfs listed in the SDSS DR7 spectroscopic catalogue (Kleinman et al. 2013), meeting our photometric selection criteria and lying within 20° of a candidate binary. We modelled the distribution of these proper motions with an asymmetric pseudo-Voigt profile,⁴ normalizing this function over the range -150 to $+150$ mas yr⁻¹ on each axis (the distributions are effectively zero beyond these limits). For the probability distributions of the distance and proper motion of the secondary star, in case it is a companion white dwarf, $P(\text{dist} | C)$ and $P(\text{pm} | C)$, respectively, we adopted normalized Gaussian functions centred on the values observed for the primary component

and with widths corresponding to the uncertainties in these measurements. Similarly, for the conditional probabilities of the observed secondary star distances and proper motions, $P(\text{data} | \text{dist})$ and $P(\text{data} | \text{pm})$, we adopted normalized Gaussian functions centred on the observed values for the secondary component and with widths matching the uncertainties in those measurements

$$P(\text{data} | C) = \int_0^{1250} P(\text{data} | \text{dist})P(\text{dist} | C)d \text{dist} \\ \times \int_{-150}^{150} P(\text{data} | \text{pm})P(\text{pm} | C)d \text{pm} \quad (2)$$

$$P(\text{data} | F) = \int_0^{1250} P(\text{data} | \text{dist})P(\text{dist} | F)d \text{dist} \\ \times \int_{-150}^{150} P(\text{data} | \text{pm})P(\text{pm} | F)d \text{pm} \quad (3)$$

Subsequently, we used equations (2) and (3) to calculate $P(\text{data} | C)$ and $P(\text{data} | F)$, respectively (e.g. Kass & Raftery 1995), for each candidate binary, where the integrals were evaluated by sampling the functions at several thousand points across their respective ranges. The ratios of these parameters, as listed in the final column of Table 3, are the approximate Bayes factors of our models. For uninformative priors (i.e. $P(C) = P(F) = 0.5$), they equate to the ratios of the posterior probabilities of the two models for the secondary, $P(C|\text{data})$ and $P(F|\text{data})$. An inspection of the Bayes factors in Table 3 reveals that physical association of the components is strongly and very strongly favoured in 2 and 14 pairings, respectively, (Jeffreys 1961). Only the pair we suspected above to be non-physical, CDDS 34, is rated as more likely to be a chance alignment. Consequently, we do not consider it further in this work.

5 WIDE BINARY WHITE DWARF MASSES

5.1 The young, wide, double-degenerate mass distribution

We have expanded our sample of 16 binaries by folding in three previously known hot, wide, non-magnetic, double-degenerates that lie within the footprint of SDSS DR7. We have confirmed these to be physical systems by subjecting their components to the same analysis we performed on our new candidate binaries (see Table 4). Subsequently, we have built a mass distribution from the 38 white dwarfs of this enlarged sample (Fig. 6). This distribution is of importance because it conveys information relating to the initial mass function of the progenitor stellar population and the stellar IFMR (e.g. Ferrario et al. 2005).

While the white dwarf mass distribution has been determined several times previously, these efforts have been based on samples dominated by isolated field objects e.g. from the SDSS DR4 (Kepler et al. 2007) and from the Palomar-Green (PG; Liebert, Bergeron & Holberg 2005) surveys. These distributions are loosely described in terms of three peaks, a main one located around $M = 0.6 M_\odot$ which arises from the progeny of the numerous F dwarfs of the Galactic disc, a high-mass one centred at $M = 0.8\text{--}0.9 M_\odot$, often attributed to binary mergers (e.g. Yuan 1992) but which more recent kinematic work links to early-type stars that naturally lead to larger remnants (Wegg & Phinney 2012), and a low-mass one stationed around $M = 0.4 M_\odot$, associated with close binary evolution and the non-conservative transfer of mass (e.g. Marsh, Dhillon & Duck 1995). It is important to note that in magnitude-limited samples

⁴ www.xray.cz/xrdmlread/PseudoVoigtAsym-m

Table 4. Effective temperatures and surface gravities obtained from Koester et al. (2009) for the components of three previously identified wide DA + DA binary systems. We also list the theoretical absolute r magnitudes, the distance moduli, the masses and the proper motions for these white dwarfs.

ID	T_{eff} (K)	$\log g$ ($\log_{10}(\text{cm s}^{-2})$)	ΔM (M_{\odot})	M_r (mag)	$r - M_r$ (mag)	M (M_{\odot})	$\mu_{\alpha} \cos \delta, \mu_{\delta}$ (mas yr $^{-1}$)	$\frac{P(\text{data} \text{C})}{P(\text{data} \text{F})}$	DD?
CDDS18-A	$23\,537 \pm 541$	8.23 ± 0.07	–	$11.05^{+0.12}_{-0.12}$	5.50 ± 0.12	0.77 ± 0.04	$-49.9 \pm 9.9, -30.3 \pm 9.9$	61	✓
CDDS18-B	$25\,783 \pm 593$	9.04 ± 0.07	–	$12.39^{+0.16}_{-0.16}$	5.12 ± 0.18	1.22 ± 0.03	$-33.5 \pm 9.9, -34.0 \pm 9.9$		
CDDS49-A	$14\,601 \pm 336$	8.08 ± 0.07	–	$11.62^{+0.11}_{-0.12}$	4.58 ± 0.12	0.66 ± 0.04	$53.0 \pm 3.6, -71.1 \pm 3.6$	$\gg 10\,000$	✓
CDDS49-B	$18\,743 \pm 431$	8.24 ± 0.07	–	$11.45^{+0.12}_{-0.12}$	4.46 ± 0.12	0.77 ± 0.04	$54.0 \pm 3.6, -75.5 \pm 3.6$		
CDDS51-A	$15\,636 \pm 360$	7.86 ± 0.07	–	$11.19^{+0.11}_{-0.10}$	6.24 ± 0.11	0.54 ± 0.04	$-32.8 \pm 3.1, -69.7 \pm 3.1$	> 10000	✓
CDDS51-B	$13\,935 \pm 321$	7.99 ± 0.07	–	$11.57^{+0.11}_{-0.11}$	6.35 ± 0.13	0.60 ± 0.04	$-31.3 \pm 3.1, -74.4 \pm 3.1$		

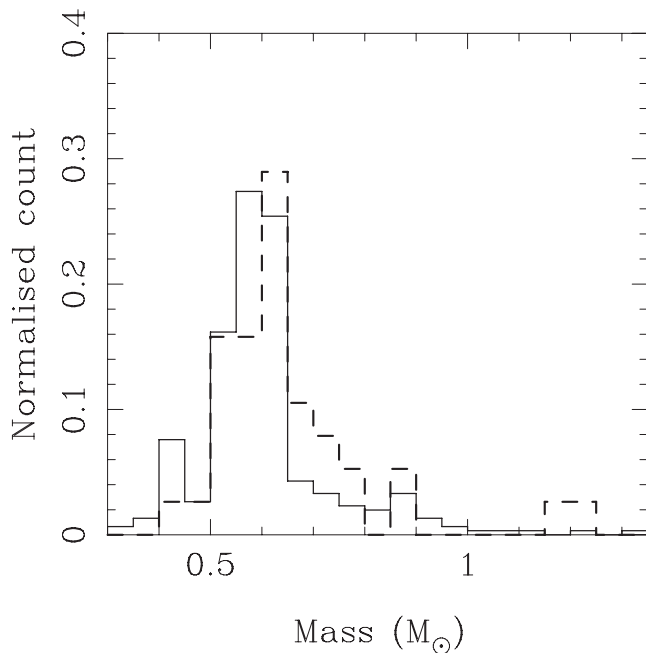


Figure 6. Normalized mass distribution for our binary white dwarf sample (heavy dashed line). The normalized mass distribution for the 303 white dwarfs with $T_{\text{eff}} > 12\,000$ K in the Palomar-Green survey is overplotted (thin solid line).

such as those from the PG and the SDSS DR4 surveys, low- and high-mass white dwarfs are over- and underrepresented due to their greater and lesser than average intrinsic luminosities, respectively (e.g. see Liebert et al. 2005, for discussion).

It is apparent from Fig. 6 that the mass distribution of our largely magnitude-limited sample of young, wide double-degenerates, also displays a strong peak around $0.6 M_{\odot}$. Indeed, we find the mean masses of the 300 PG white dwarfs with $T_{\text{eff}} > 12\,500$ K (we exclude PG0922+162 and do not attempt to apply our mass corrections at lower temperatures since Liebert et al. used a previous generation of synthetic spectra) and ours, $0.60 M_{\odot}$ and $0.65 M_{\odot}$, respectively, to be comparable. Some of the small difference in these means is likely attributable to our use of more modern synthetic H-line profiles (see e.g. Tremblay et al. 2011) although unlike the mass distribution of the PG white dwarfs, where there is a prominent peak around $0.4 M_{\odot}$ and 37 objects with $M < 0.5 M_{\odot}$, our binary sample harbours only two objects with masses that are likely to be $M < 0.5 M_{\odot}$. From drawing 10 000 random subsamples of 38 white dwarfs from the PG sample, we estimate the likelihood of

there being two or fewer objects with $M < 0.5 M_{\odot}$ in our sample as $P \sim 0.2$, suggesting that, for now, the observed shortfall is not significant. A relative deficit of low-mass objects might become apparent in a larger wide, double-degenerate sample because it is likely that low-mass products of close binary evolution located in triple-degenerate systems will generally be partnered in wider orbits by white dwarfs of canonical mass. These have smaller radii and are intrinsically fainter, reducing the influence of the luminosity bias that operates in favour of the detection of low-mass white dwarfs in isolated samples.

Following the same Monte Carlo approach applied above, we find the presence of two white dwarfs amongst our 19 binaries (CDDS 18-B and CDDS 26-A), which sit well above recent theoretical predictions for the minimum mass of ONe core degenerates (e.g. $M \sim 1.05\text{--}1.1 M_{\odot}$; Gil-Pons et al. 2003; Siess 2007) to represent a significant excess ($P \sim 0.05$). In the PG sample, only 3 out of 300 objects have masses this large. The formation of ultramassive white dwarfs remains a matter of some debate since it is unclear if the putative single super-AGB progenitor stars ($M_{\text{init}} > 6 M_{\odot}$; e.g. Eldridge & Tout 2004; Bertelli et al. 2009) lose their envelopes sufficiently rapidly to prevent their degenerate cores growing until they detonate as electron capture supernovae. Although the ultramassive field degenerate GD 50 has been linked with the recent Pleiades star formation event (Dobbie et al. 2006b), it is intriguing that no white dwarfs with masses as large as these two objects have yet been unearthed within open clusters (Dobbie et al. 2012b; Williams, Bolte & Koester 2009). Considering their masses are distinctly similar to the sum of the masses of two objects from the main peak in the mass distribution, alternatively, these white dwarfs might have formed through double-degenerate merging (e.g. Vennes et al. 1997). While this putative merging process would likely lead to discord between the cooling times of the components of these two systems (e.g. see the discussion relating to RE J0317-853; Barstow et al. 1995; Ferrario et al. 1997; Burleigh, Jordan & Schweizer 1999; Külebi et al. 2010), the fundamental parameters of PG 0922+162A and PG 0922+162B (CDDS 18) appear to fit entirely within the framework of standard stellar evolution (see Section 6). In the case of CDDS26, coherence between the component cooling times is less satisfactory but there is no overwhelming disparity which flags a more exotic evolutionary history for CDDS26-A.

More broadly, it is of interest that the majority of the higher mass stars in our binary sample are paired with each other. The simplest explanation for this favours these objects being the progeny of early-type stars. The white dwarfs within the peak of the mass distribution are typically the end points of stars which have reasonably long lives on the main sequence (at least several Gyr). The bulk of companion (higher mass) white dwarfs originating from early-type stars with

relatively short main-sequence lifetimes will have cooled below $T_{\text{eff}} \approx 8000\text{--}9000\text{ K}$ (e.g. 2.5 Gyr for $0.9 M_{\odot}$) and moved out with our colour selection region prior to the formation of a double-degenerate system. It is widely documented that stars of greater mass are more likely to reside in multiple systems than those of lower mass. The binary fraction for the lowest mass M dwarfs is estimated to be only 25–35 per cent (e.g. Reid & Gizis 1997; Delfosse et al. 2004), while it is found to be around 70 per cent for the O and B stars (e.g. Mason et al. 1998; Sana et al. 2008). However, as the binary fraction of the F- and G-type stars (the progeny of which dominate the white dwarf mass distribution) is only slightly lower than this at 50–60 per cent (Abt & Levy 1976; Duquenois & Mayor 1991), it seems unlikely that gross variations in the binary fraction with stellar mass can account for the excess of very high mass degenerates in our study. Alternatively, it could have arisen because the projected separation distribution of companions to early-type stars like the progenitors of these white dwarfs is peaked at several hundred au compared to a few tens of au, as for stars of later spectral type (Patience et al. 2002; De Rosa et al. 2014). During the final stages of stellar evolution, when the orbits widened, following Jean’s theorem (e.g. Iben 2000), those of the intermediate-mass stars expanded by around a factor 5–10 while those of the F/G stars grew significantly less, leaving the peak of the latter systems at or below the resolution limit of the SDSS imaging data. This may have been further compounded by the bulk of the near-equal-mass progenitor systems, where both components can evolve beyond the main sequence within a Hubble time, populating the lower half of the projected separation distribution (De Rosa et al. 2014).

5.2 Applying the non-magnetic binary sample to probe the origins of unusual white dwarfs: the HFMWDs

Around 10 per cent of white dwarfs have a magnetic field with $B > 1\text{ mG}$, the HFMWDs. Those with H-rich atmospheres (the majority) are identified from Zeeman splitting of the pressure broadened Balmer lines in their optical spectrum. However, the standard spectral technique applied to determine non-magnetic white dwarf masses (e.g. Bergeron, Saffer & Liebert 1992) does not work well for HFMWDs due to poor understanding of the broadening from the interaction of the electric and magnetic fields at the atomic scale. Consequently, mass estimates are available for relatively few HFMWDs and often have large uncertainties. They reveal these objects to be generally more massive ($\Delta M \sim 40$ per cent) than their non-magnetic cousins (e.g. Wickramasinghe & Ferrario 2005; Kepler et al. 2013). The difficulties in determining the parameters of HFMWDs, in particular their ages, also mean that assessing their origins is problematic.

Short of a detailed statistical analysis of the kinematics of a large sample of hot white dwarfs, age information can only be readily accessed for HFMWDs that are members of open clusters or specific types of wide binary systems. During the course of this work, we have unearthed several new hot, wide, magnetic + non-magnetic double-degenerate systems (Dobbie et al. 2012a, 2013, Dobbie et al. in preparation). For each system, we have compared our estimate of the mass of the non-magnetic component to recent determinations of the stellar IFMR to infer a progenitor mass. This has been matched to a grid of solar metallicity stellar evolutionary models to determine the stellar lifetime (Girardi et al. 2000). Subsequently, we have linearly combined this with the cooling time of the white dwarf to obtain a limit on the total age of the binary and ultimately a lower limit on the mass of the companion HFMWD’s progenitor.

However, any selection effects imprinted on our young, wide, double-degenerate sample, as discussed above, could potentially lead to biased conclusions about the progenitors of HFMWDs, if these systems are examined only in isolation. The two main competing hypothetical pathways to the formation of HFMWDs should synthesize them on different time-scales since stellar lifetimes are strongly mass dependent. For example, if they descend primarily from magnetic Ap/Bp stars ($M_{\text{init}} \gtrsim 2 M_{\odot}$; e.g. Angel, Borra & Landstreet 1981), then most will be formed within only a few hundred Myr (i.e. lifetimes of early-F, A and B stars) after the birth of their host population. Alternatively, if their magnetism is generated by differential rotation within gas which envelopes primordial close binaries, either when their primary stars ($M_{\text{init}} \geq 0.8 M_{\odot}$) expand to giant scale and overflow their Roche lobes (Tout et al. 2008; Nordhaus et al. 2011) or during merging of two degenerate remnants (García-Berro et al. 2012), the majority of HFMWDs, like field white dwarfs, will be created several Gyr after the birth of their progenitor stars (i.e. form mainly from the numerically dominant F and G stars). The mass distribution of any wide degenerate companions to HFMWDs, when compared to that of the non-magnetic + non-magnetic white dwarf systems, could provide insight on the lifetimes of the progenitor stars and thus clues as to which of these formation pathways is more dominant.

An examination of the component masses in our 19 systems reveals that in 13 cases both are $M < 0.7 M_{\odot}$. In contrast, out of seven known hot, wide, magnetic + non-magnetic double-degenerates, only one harbours a non-magnetic white dwarf with $M < 0.7 M_{\odot}$ (that is the five systems discussed in Dobbie et al. 2013, and two more reported in Dobbie et al. in preparation, in which the non-magnetic DA components have masses of $0.76 \pm 0.06 M_{\odot}$, CDDS 22-A, and $0.56 \pm 0.04 M_{\odot}$, CDDS 27-A). While the masses of the HFMWDs in these seven binaries may well have been modified through stellar interactions, the masses of the non-magnetic DA companions are presumably reflective of the spectral types of their progenitor stars. Unless some factor has dictated otherwise (e.g. the evolutionary time-scales for the formation of the HFMWDs), the progenitor stars of these white dwarfs should have had the same broad distribution in mass as those of the components of the 19 non-magnetic + non-magnetic double-degenerate binaries studied here. Adopting this as a null hypothesis, we have drawn thousands of subsets of seven degenerates randomly from the 19 non-magnetic binary systems. We find that only approximately 10 (100) subsamples per 10 000 contain six (five) white dwarfs with $M \geq 0.7 M_{\odot}$. We have also applied a two-sample Kolmogorov–Smirnov test to the mass distributions of the seven non-magnetic companions and the more massive white dwarf components in each of our 19 binaries. For $n_1 = 7$ and $n_2 = 19$, the critical D_{crit} values are 0.54 and 0.60 for $P = 0.1$ and $P = 0.05$, respectively. From the cumulative distributions shown in Fig. 7, we determine $D = 0.54$, which rejects at marginal significance the null hypothesis. These findings suggest these two groups of white dwarfs may have different progenitor mass distributions.

This disparity in these two mass distributions favours a formation model in which the origins of HFMWDs preferentially involve early-type stars, although it does not categorically rule out the hypothesis that they form as a result of stellar interaction. For example, it is possible they are born from higher order stellar systems. Studies of main-sequence stars reveal a non-negligible proportion of binaries are in fact higher order systems, principally triples (~ 25 per cent; Raghavan et al. 2010). For reasons of dynamical stability, the majority of these systems are structured hierarchically, such that they consist of a relatively close (and potentially interacting)

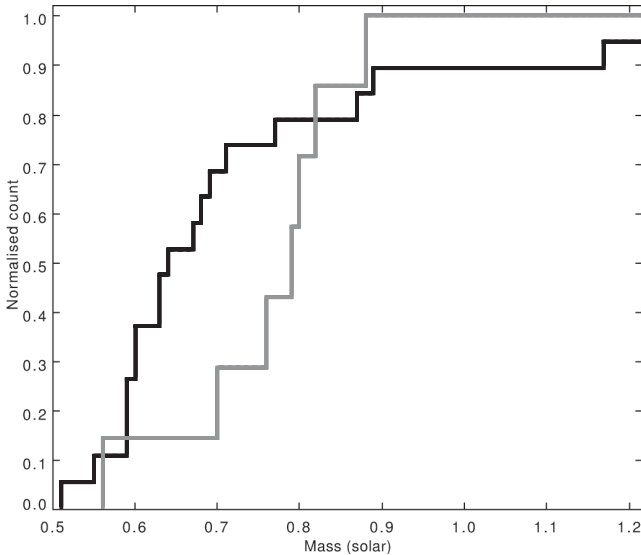


Figure 7. Normalized cumulative mass distribution for our binary white dwarf sample (black line). The normalized cumulative mass distribution for the seven DA white dwarfs in magnetic + non-magnetic systems is overplotted (grey line).

pair with a tertiary companion in a much wider orbit (e.g. Black 1982; Tokovinin 1997). Our result would, however, require stars of earlier spectral type to occur more frequently in higher order multiple systems. Moreover, as current understanding of the IFMR indicates that stars of earlier spectral-type naturally lead to more massive white dwarfs, there is less need in this case to invoke merging to account for the larger than average masses of HFMWDs. Admittedly, our findings appear difficult to reconcile with the almost complete absence of HFMWDs in the more than 2000 close, detached white dwarf + main-sequence binaries known to date (e.g. Rebassa-Mansergas et al. 2012; Parsons et al. 2013), particularly considering the existence of a healthy population of magnetic cataclysmic variables. Precision kinematics for large numbers of hot, recently formed, field white dwarfs from *Gaia* (Jordan 2008) will provide a crucial complementary view on the origins of HFMWDs. For now, spectroscopic studies of additional young, wide, double-degenerate systems would be useful to strengthen or refute the trend discussed above. For example, our initial work could be extended to include objects from the most recent SDSS coverage and regions of sky explored by the SkyMapper (Keller et al. 2007) and VST ATLAS (Shanks & Metcalfe 2012) surveys.

6 THE NON-MAGNETIC BINARY SAMPLE AND THE IFMR

Our current knowledge about the form of the fundamentally important stellar IFMR is derived predominantly from observations of white dwarfs that are members of open clusters. Most open cluster studies of the IFMR are consistent with a monotonic relation with a mild degree of scatter (e.g. Kalirai et al. 2008; Casewell et al. 2009; Williams et al. 2009). Only a modest number of these objects are known to deviate substantially from the general trend (e.g. LB 5893, LB 390 in nearby Praesepe cluster; Reid 1996; Casewell et al. 2009). However, potentially the open cluster data could have furnished us with a biased perspective on the form of the relation. While these data now span a comparatively broad range of initial mass ($M_{\text{init}} \approx 1.5\text{--}6 M_{\odot}$), they are still heavily concentrated

between $M_{\text{init}} = 2.8\text{--}5 M_{\odot}$. Moreover, faint candidate white dwarf members of these populations are generally identified from their location towards the blue side of colour–magnitude diagrams. Due to the premium on 8 m class telescope time any photometrically outlying cluster white dwarfs e.g. cooler, redder objects located closer to the field star population, are arguably less likely to be targeted for follow-up spectroscopic observations. Studies of white dwarfs in wide binary systems with subgiant and main-sequence stars suggest that there may be more scatter in the IFMR than indicated by the cluster work (Catalán et al. 2008; Zhao et al. 2012; Liebert et al. 2013).

Although our investigation of wide double-degenerate systems cannot provide data points with the absolute age calibration necessary for investigating the IFMR in the style of studies of open cluster white dwarfs or white dwarf + subgiant binaries, they can still serve as a useful test of its relative form. Hence, we have derived the cooling time for each of our binary white dwarfs, including the DB, with the mixed CO core composition ‘thick H-layer’ evolutionary calculations of the Montreal Group (Fontaine, Brassard & Bergeron 2001, the cooling time of the DB is largely insensitive to our choice of H-layer mass). The errors on our estimates are derived by propagating the uncertainties in effective temperature and surface gravity. We have applied three relatively recent, linear model estimates of the IFMR and grids of solar metallicity stellar evolutionary models (Girardi et al. 2000) to infer both the masses and the stellar lifetimes of the white dwarfs’ progenitor stars. These IFMRs have been derived by different research teams (Dobbie et al. 2006a; Kalirai et al. 2008; Williams et al. 2009) and do not include white dwarfs with $T_{\text{eff}} < 12\,500$ K, the masses of which can be systematically overestimated (e.g. see Kepler et al. 2007). Next, we have combined these lifetimes with the degenerate cooling times to obtain two independent determinations of the total age of each system for each assumed IFMR. Finally, we have calculated the differences between these pairs of age estimates. For negligible measurement errors and a perfect model of a monotonic IFMR with no intrinsic scatter, these should be zero. The uncertainties associated with these values have been determined following a Monte Carlo approach.

Examination of the age discrepancies in Table 5 reveals that importantly, none of the 19 systems is strongly discordant with our current understanding of the form of the IFMR. The deviations from zero or no age difference are within 1σ for 11 out of the 19 systems and less than about 2.1σ for the remaining binaries, suggesting that the dominant contributors to the non-zero values are the uncertainties on our parameter estimates. Unfortunately, these are generally large, especially at lower initial masses. This is where the inferred main-sequence lifetime is, in an absolute sense, a strong function of mass, curbing the usefulness of these systems for this work. For initial masses $M_{\text{init}} \gtrsim 2.5 M_{\odot}$, the uncertainties are typically only a few 100 Myr and the parameters of the bulk of systems here can be comfortably reconciled with any of the three model IFMRs. This is perhaps not surprising as the data around which these models are constructed is drawn primarily from $M_{\text{init}} \gtrsim 2.5 M_{\odot}$. Third dredge-up is also anticipated to be rather efficient in this mass regime at preventing further growth of the degenerate core during thermally pulsing asymptotic giant branch evolution (e.g. see discussion in Weidemann 2000). Any factor that can substantially interfere with the mass-loss process at this time, when the radius of a star reaches its maximum (e.g. the presence of a close companion) is likely to have a relatively minor impact on the final remnant mass. In comparison, at lower initial mass, third dredge-up is anticipated to be less efficient, potentially allowing the core to grow significantly during this phase. Differences in third dredge-up efficiency, as a function on

Table 5. Progenitor masses for the white dwarfs, determined from three recent estimates of the form of the IFMR, 1. Dobbie et al. (2006a), 2. Kalirai et al. (2008) and 3. Williams et al. (2009). Stellar lifetimes have been derived from the solar metallicity evolutionary models of Girardi et al. (2000). We have calculated the difference between the system age derived from component A and the system age derived from component B. This should be zero for negligible measurement errors and a perfect representation of a monotonic IFMR with no intrinsic scatter. Where an uncertainty is listed as HT, the calculated error bound extends to or lies beyond a Hubble time. When both bounds are larger than a Hubble time, we flag the estimate as providing no meaningful constraint (NMC). The projected separation of the components of each system are also shown (rounded to 25 au).

Component	IFMR 1		IFMR 2		IFMR 3		Separation /au
	$M_{\text{init}}/M_{\odot}$	$\Delta\text{System age/Myr}$	$M_{\text{init}}/M_{\odot}$	$\Delta\text{System age/Myr}$	$M_{\text{init}}/M_{\odot}$	$\Delta\text{System age/Myr}$	
CDDS3-A	$2.25^{+0.59}_{-0.52}$	-901^{+689}_{-2446}	$1.78^{+0.46}_{-0.41}$	$-2733^{+3095}_{\text{HT}}$	$1.93^{+0.34}_{-0.31}$	-1419^{+1369}_{-5973}	1725
CDDS3-B	$1.89^{+0.67}_{-0.60}$		$1.34^{+0.63}_{-0.59}$		$1.56^{+0.50}_{-0.47}$		
CDDS6-A	$2.87^{+0.63}_{-0.55}$	-155^{+236}_{-276}	$2.54^{+0.48}_{-0.46}$	-216^{+463}_{-546}	$2.57^{+0.35}_{-0.34}$	-188^{+368}_{-412}	400
CDDS6-B	$2.74^{+0.63}_{-0.54}$		$2.39^{+0.48}_{-0.45}$		$2.44^{+0.36}_{-0.34}$		
CDDS8-A	$2.62^{+0.61}_{-0.52}$	-630^{+291}_{-515}	$2.23^{+0.45}_{-0.42}$	-736^{+711}_{-1330}	$2.31^{+0.33}_{-0.30}$	-682^{+513}_{-755}	3225
CDDS8-B	$2.53^{+0.71}_{-0.62}$		$2.13^{+0.63}_{-0.60}$		$2.22^{+0.50}_{-0.48}$		
CDDS9-A	$1.33^{+0.79}_{-0.73}$	3380^{HT}_{-3157}	<1.49	NMC	$0.99^{+0.68}_{-0.65}$	$11605^{\text{HT}}_{-12393}$	5875
CDDS9-B	$2.29^{+0.70}_{-0.62}$		$1.83^{+0.64}_{-0.60}$		$1.97^{+0.51}_{-0.48}$		
CDDS14-A	$2.35^{+0.69}_{-0.61}$	-618^{+769}_{-1478}	$1.91^{+0.62}_{-0.58}$	-1250^{+2485}_{-11131}	$2.04^{+0.49}_{-0.47}$	-671^{+1143}_{-3637}	1075
CDDS14-B	$2.06^{+0.70}_{-0.64}$		$1.55^{+0.66}_{-0.63}$		$1.74^{+0.53}_{-0.51}$		
CDDS15-A	$1.67^{+0.64}_{-0.59}$	245^{+3872}_{-2081}	$1.08^{+0.59}_{-0.58}$	NMC	$1.34^{+0.47}_{-0.47}$	180^{HT}_{-5726}	725
CDDS15-B	$1.66^{+0.53}_{-0.48}$		$1.06^{+0.42}_{-0.39}$		$1.33^{+0.31}_{-0.30}$		
CDDS16-A	<2.86	NMC	<2.45	NMC	<2.52	NMC	1850
CDDS16-B	$1.60^{+0.85}_{-0.72}$		$0.99^{+0.92}_{-0.78}$		$1.26^{+0.75}_{-0.65}$		
CDDS17-A	$3.19^{+0.92}_{-0.85}$	-273^{+508}_{-809}	$2.93^{+1.02}_{-0.99}$	-834^{+1043}_{-3731}	$2.90^{+0.73}_{-0.74}$	-639^{+830}_{-1377}	900
CDDS17-B	$2.30^{+0.71}_{-0.64}$		$1.85^{+0.67}_{-0.65}$		$1.99^{+0.53}_{-0.52}$		
CDDS18-A	$3.60^{+0.70}_{-0.60}$	46^{+172}_{-98}	$3.42^{+0.52}_{-0.49}$	96^{+167}_{-100}	$3.32^{+0.37}_{-0.36}$	114^{+128}_{-87}	525
CDDS18-B	$7.00^{+1.01}_{-0.84}$		$7.58^{+0.61}_{-0.58}$		$6.83^{+0.31}_{-0.33}$		
CDDS26-A	$6.65^{+0.98}_{-0.81}$	-1535^{+914}_{-5286}	$7.15^{+0.62}_{-0.57}$	$-6256^{+4920}_{\text{HT}}$	$6.47^{+0.34}_{-0.34}$	$-3163^{+1842}_{\text{HT}}$	725
CDDS26-B	$1.76^{+0.66}_{-0.61}$		$1.18^{+0.62}_{-0.60}$		$1.42^{+0.49}_{-0.47}$		
CDDS29-A	$4.34^{+0.78}_{-0.66}$	-72^{+107}_{-204}	$4.33^{+0.57}_{-0.53}$	-176^{+142}_{-250}	$4.08^{+0.40}_{-0.38}$	-164^{+120}_{-180}	825
CDDS29-B	$3.22^{+0.68}_{-0.58}$		$2.96^{+0.53}_{-0.48}$		$2.93^{+0.37}_{-0.36}$		
CDDS30-A	$1.61^{+0.66}_{-0.60}$	946^{+6381}_{-1472}	$1.01^{+0.61}_{-0.59}$	NMC	$1.28^{+0.48}_{-0.47}$	5495^{HT}_{-3009}	425
CDDS30-B	$1.97^{+0.67}_{-0.61}$		$1.44^{+0.62}_{-0.59}$		$1.64^{+0.49}_{-0.47}$		
CDDS31-A	$4.52^{+0.78}_{-0.68}$	192^{+101}_{-179}	$4.55^{+0.57}_{-0.54}$	116^{+129}_{-213}	$4.27^{+0.39}_{-0.39}$	118^{+116}_{-165}	150
CDDS31-B	$3.37^{+0.68}_{-0.59}$		$3.15^{+0.53}_{-0.48}$		$3.09^{+0.38}_{-0.36}$		
CDDS36-A	$2.24^{+0.59}_{-0.51}$	-313^{+574}_{-663}	$1.77^{+0.46}_{-0.42}$	-775^{+1756}_{-3328}	$1.93^{+0.34}_{-0.31}$	-331^{+820}_{-1343}	4025
CDDS36-B	$2.08^{+0.58}_{-0.50}$		$1.57^{+0.45}_{-0.41}$		$1.76^{+0.33}_{-0.31}$		
CDDS40-A	$2.33^{+0.68}_{-0.62}$	138^{+724}_{-393}	$1.88^{+0.61}_{-0.60}$	592^{+2770}_{-869}	$2.02^{+0.49}_{-0.48}$	437^{+1123}_{-695}	2100
CDDS40-B	$2.92^{+0.72}_{-0.65}$		$2.60^{+0.64}_{-0.61}$		$2.62^{+0.49}_{-0.49}$		
CDDS48-A	$3.05^{+0.73}_{-0.66}$	36^{+293}_{-397}	$2.75^{+0.64}_{-0.62}$	-294^{+640}_{-633}	$2.75^{+0.49}_{-0.50}$	-135^{+470}_{-467}	475
CDDS48-B	$2.54^{+0.61}_{-0.53}$		$2.13^{+0.48}_{-0.44}$		$2.23^{+0.35}_{-0.34}$		
CDDS49-A	$2.78^{+0.64}_{-0.55}$	401^{+337}_{-194}	$2.43^{+0.50}_{-0.46}$	623^{+554}_{-325}	$2.48^{+0.36}_{-0.35}$	550^{+381}_{-255}	525
CDDS49-B	$3.58^{+0.70}_{-0.61}$		$3.41^{+0.53}_{-0.50}$		$3.31^{+0.38}_{-0.38}$		
CDDS50-A	$2.57^{+0.62}_{-0.54}$	-347^{+360}_{-663}	$2.17^{+0.49}_{-0.45}$	-551^{+876}_{-2327}	$2.26^{+0.36}_{-0.34}$	-509^{+687}_{-1017}	375
CDDS50-B	$2.37^{+0.70}_{-0.62}$		$1.93^{+0.63}_{-0.59}$		$2.06^{+0.50}_{-0.48}$		
CDDS51-A	$1.86^{+0.55}_{-0.48}$	618^{+1561}_{-594}	$1.31^{+0.43}_{-0.41}$	2800^{HT}_{-2540}	$1.54^{+0.32}_{-0.31}$	1265^{+2768}_{-1119}	2200
CDDS51-B	$2.37^{+0.60}_{-0.51}$		$1.93^{+0.47}_{-0.43}$		$2.06^{+0.35}_{-0.33}$		

main-sequence mass, might explain some of the additional scatter reported in previous wide binary studies of the IFMR. These tend to sample lower initial masses. However, some of the extra dispersion in the results of these studies undoubtedly stems from the neglect of the spectroscopic overestimate of mass at $T_{\text{eff}} < 12\,000$ K.

7 ADDITIONAL NOTES ON SOME SPECIFIC SYSTEMS

7.1 CDDS15

All new white dwarfs presented here have hydrogen dominated atmospheres, except CDDS15-A which is a DB. Following L151-81A/B (Oswalt, Hintzen & Luyten 1988), CDDS15 is only the second wide DA + DB system identified to date. However, a number of unresolved, presumably close, DA + DB systems are also known or suspected, including MCT 0128-3846, MCT 0453-2933 (Wesemael et al. 1994), PG 1115+166 (Bergeron & Leggett 2002; Maxted et al. 2002) and KUV 02196+2816 (Limoges, Bergeron & Dufour 2009). The latter two systems have total system masses close to the Chandrasekar limit ($1.4 M_{\odot}$) but although PG 1115+166 is also known to be a post-common-envelope binary its components are too widely separated ($a \sim 0.2$ au) for it to merge within a Hubble time. CDDS15-A and CDDS15-B are both located on the lower side of the peak in the field white dwarf mass distribution and have relatively large tangential velocities ($v_{\text{tan}} \approx 90$ km s $^{-1}$). D’Antona & Mazzitelli (1991) have suggested that DBs preferentially form for lower mass progenitors ($M_{\text{init}} < 2 M_{\odot}$) where the very high mass-loss rates experienced at the peak of the last thermal pulse cycle can remove the entire hydrogen surface envelope in a very short time. However, at least one helium-rich white dwarf is known which must, because of its membership of the 625 Myr Hyades cluster, have descended from a star with $M_{\text{init}} > 2 M_{\odot}$. L151-81A also appears likely to be the progeny of a moderately early-type star since from its higher than average mass ($M = 0.71 M_{\odot}$) hydrogen-rich degenerate companion, L151-81B ($T_{\text{eff}} = 10\,460$ K, $\log g = 8.43$; Gianninas, Bergeron & Ruiz 2011), we infer an upper limit of $\tau \lesssim 2$ Gyr on the age of this system. This corresponds to the lifetime of a $M_{\text{init}} \gtrsim 1.7 M_{\odot}$ star. Interestingly, spectroscopic surveys of large samples of field white dwarfs have also found the mean mass of the DBs to be significantly larger than that of the DA population (e.g. $\bar{M}_{\text{DB}} = 0.67 M_{\odot}$ and $\bar{M}_{\text{DA}} = 0.63 M_{\odot}$; Bergeron et al. 2011; Gianninas et al. 2011). In a spectroscopic analysis of 140 DBs ($T_{\text{eff}} > 16\,000$ K) drawn from the SDSS DR7, Kleinman et al. (2013) found only one with $M < 0.55 M_{\odot}$. Similarly, in a study of 108 relatively bright DBs, Bergeron et al. (2011) also found only one with a mass this low. It seems that CDDS15-A is perhaps slightly unusual for its rather low mass. The construction and the investigation of the properties (e.g. separation and companion mass distributions) of a sample of wide DA + DB binaries would likely provide additional insight on the evolutionary pathway that leads to the formation of hydrogen-deficient degenerates.

7.2 CDDS30

The components of CDDS30 are separated by approximately 2.8 arcsec, which translates to around 400 au at the distance we calculate for this system. It is unlikely that these two objects have ever exchanged mass via Roche lobe overflow, so their masses, which are consistent with the lower side of the peak in the field white dwarf mass distribution, suggest that they are the progeny of main-sequence stars that had comparatively modest masses ($M < 2 M_{\odot}$).

We note that this pairing is only 16 arcsec (2400 au at 150 pc) from a relatively bright ($B = 13.17$, $V = 12.12$, $J = 10.37 \pm 0.02$, $H = 9.94 \pm 0.03$, $K_s = 9.82 \pm 0.02$), late-type star, TYC 2535-524-1, which the Tycho-2 catalogue (Høg et al. 2000) reveals has a similar proper motion ($\mu_{\alpha} \cos \delta = -44.3 \pm 3.5$ mas yr $^{-1}$, $\mu_{\delta} = 30.6 \pm 3.5$ mas yr $^{-1}$). Motivated by this, we have performed a crude estimate of the distance to this star. The optical colours drawn from the American Association of Variable Star Observers Photometric All Sky Survey (<http://www.aavso.org/apass>) appear to be consistent with a spectral type of K3–K4 (e.g. HD 219134, TW Piscis Austri). The near-IR colours from 2MASS are indicative of spectral types K2–K3 (e.g. ϵ -Eridani, HD 219134). We are led to conclude that TYC 2535-524-1 is approximately K2–4V, which according to a recently published relation between absolute H -band magnitude and spectral type (Kirkpatrick et al. 2012), corresponds to $M_H \approx 4.0$ – 4.6 mag. From the observed H magnitude of $H = 9.94 \pm 0.03$, we derive a distance modulus of 5.3–5.9, which is in accord with that we infer for CDDS30-A and CDDS30-B. Considering the similarities between these distance estimates and the statistically significant proper motion measurements, we are led to conclude that there is a reasonable likelihood that these two white dwarfs and TYC 2535-524-1 form a triple stellar system. The mass of the main-sequence star sets a lower limit on the mass of the white dwarfs’ progenitors of $M > 0.6 M_{\odot}$. However, a detailed spectroscopic study of the early-K dwarf, including activity indicators, may provide limits on the total age of this system (e.g. Mamajek & Hillenbrand 2008) that can lead to better constraints on the progenitor masses.

7.3 CDDS 8-A and other possible ZZ Ceti stars

At least one system in our survey harbours a white dwarf that has been confirmed previously as a pulsating ZZ Ceti star. CDDS 8-A (SDSS J033236.61–004918.4) was first reported as a DA in the catalogue of spectroscopically identified white dwarfs compiled from the first release of the SDSS data (Kleinman et al. 2004). It was subsequently shown to be lying within the instability strip and pulsating with an amplitude of 15.1 mma on a period of 767.5 s (Mukadam et al. 2004). As referred to in Section 4.1, we find a discrepancy of several hundred K between the effective temperature we measure for this object and that reported by Kleinman et al. (2013). It is known that systematic uncertainties of this magnitude in spectroscopic estimates of the atmospheric parameters of ZZ Ceti white dwarfs can arise if the data are not averaged over several pulsation cycles (e.g. see Gianninas et al. 2011). Our VLT observations of this object spanned only 1200 s, corresponding to less than two cycles of the presumably most prominent pulsation mode reported by Mukadam et al. (2004). The two distinct SDSS spectra of this star also hint at variability in the shape and location of the $H\alpha$ line core. This effect is likely due to velocity fields within the photosphere that result from the pulsational motion (Koester & Kompas 2007).

Considering CDDS 8-A lies on the red edge of the instability strip and has an extremely bright, hot, white dwarf companion, SDSS J033236.86–004936.9 (Noguchi, Maehara & Kondo 1980; Wegner, McMahan & Boley 1987; McCook & Sion 1999), from which the distance to and kinematics of this system can be stringently constrained, it represents a particularly interesting system for further study. Aficionados of pulsating white dwarfs may be interested in a further 10 components within our spectroscopic subsample that we have flagged here on the basis of their effective temperatures as either possible (CDDS 3-A, CDDS 15-B, CDDS 16-A, CDDS 17-B, CDDS 34-B, CDDS 40-A), probable (CDDS 29-A, CDDS 48-A,

CDDS 50-A) or highly probable (CDDS 14-A) ZZ Ceti stars. A significant proportion of these objects are brighter than $g = 18$ so could be studied in more detail on telescopes of relatively modest aperture.

8 SUMMARY

We have presented spectroscopy for the components of 18 candidate young, wide, double-degenerates photometrically identified within the footprint of the SDSS DR7. On the basis of our distance estimates and our astrometry, we have concluded that 16 candidates probably form physical systems. One of these is a wide DA + DB binary, only the second such system identified to date. We have determined the effective temperatures, surface gravities, masses and cooling times of the components of our 16 binaries. We have combined the sample with three similar systems previously known from the literature to lie within the DR7 footprint to construct a mass distribution for 38 white dwarfs in young, wide double-degenerate binaries. A comparison between this and the mass distribution of the isolated field white dwarf population reveals them to have broadly similar forms, each with a substantial peak around $M \sim 0.6 M_{\odot}$. However, there is a slight excess of the most massive white dwarfs in the binary sample which could be related to the primordial separation distribution of the progenitor systems and the expansion of binary orbits during the late stages of stellar evolution. We have shown how our sample can be exploited to probe the origins of unusual white dwarfs and found at marginal significance that the progenitor systems HFMDs are preferentially associated with early-type stars, at least within these pairings. Finally, we have used the 19 young, wide double-degenerate systems to test the stellar IFMR. Within the relatively large uncertainties, no system appears to be strongly discordant with our current understanding of the relation.

ACKNOWLEDGEMENTS

This work is based in part on observations made with the Gran Telescopio Canarias (GTC), operated on the island of La Palma in the Spanish Observatorio del Roque de los Muchachos of the Instituto de Astrofísica de Canarias. The INT and the WHT are operated by the Isaac Newton Group in the Spanish Observatorio del Roque de los Muchachos of the Instituto de Astrofísica de Canarias. Based in part on observations made with ESO Telescopes at the La Silla Paranal Observatory under programme numbers 084.D-1097 and 090.D-0140. Based in part on observations obtained as part of the VISTA Hemisphere Survey, ESO Program, 179.A-2010 (PI: McMahon). This research was made possible through the use of the AAVSO Photometric All-Sky Survey (APASS), funded by the Robert Martin Ayers Sciences Fund. This research has made use of the SIMBAD data base, operated at the Centre de Données Astronomiques de Strasbourg (CDS), and of NASA's Astrophysics Data System Bibliographic Services (ADS). Funding for the SDSS and SDSS-II was provided by the Alfred P. Sloan Foundation, with Participating Institutions, the National Science Foundation, the US Department of Energy, the National Aeronautics and Space Administration, the Japanese Monbukagakusho, the Max Planck Society, and the Higher Education Funding Council for England. The SDSS website is <http://www.sdss.org/>. SDSS is managed by the Astrophysical Research Consortium for the Participating Institutions. NL acknowledges support from the national programme number AYA2010-19136 funded by the Spanish Ministry of Science and

Innovation. NL is a Ramón y Cajal fellow at the IAC (number 08-303-01-02). Balmer/Lyman lines in the DA models were calculated with the modified Stark broadening profiles of Tremblay & Bergeron (2009), kindly made available by the authors. We thank the referee for a constructive report which has improved this paper.

REFERENCES

- Abazajian K. N. et al., 2009, *ApJS*, 182, 543
 Abt H. A., Levy S. G., 1976, *ApJS*, 30, 273
 Andrews J. J., Agüeros M. A., Belczynski K., Dhital S., Kleinman S. J., West A. A., 2012, *ApJ*, 757, 170
 Angel J. R. P., Borra E. F., Landstreet J. D., 1981, *ApJS*, 45, 457
 Barbaro G., Pigatto L., 1984, *A&A*, 136, 355
 Barstow M. A., Jordan S., O'Donoghue D., Burleigh M. R., Napiwotzki R., Harrop-Allin M. K., 1995, *MNRAS*, 277, 971
 Baxter R., 2011, PhD thesis, Macquarie Univ.
 Bergeron P., Leggett S. K., 2002, *ApJ*, 580, 1070
 Bergeron P., Saffer R. A., Liebert J., 1992, *ApJ*, 394, 228
 Bergeron P., Wesemael F., Beauchamp A., 1995, *PASP*, 107, 1047
 Bergeron P. et al., 2011, *ApJ*, 737, 28
 Bertelli G., Nasi E., Girardi L., Marigo P., 2009, *A&A*, 508, 355
 Bertin E., Arnouts S., 1996, *A&AS*, 117, 393
 Black D. C., 1982, *AJ*, 87, 1333
 Burleigh M. R., Jordan S., Schweizer W., 1999, *ApJ*, 510, L37
 Casali M. et al., 2007, *A&A*, 467, 777
 Casewell S. L., Dobbie P. D., Napiwotzki R., Burleigh M. R., Barstow M. A., Jameson R. F., 2009, *MNRAS*, 395, 1795
 Casewell S. L. et al., 2012, *ApJ*, 759, L34
 Catalán S., Isern J., García-Berro E., Ribas I., Allende Prieto C., Bonanos A. Z., 2008, *A&A*, 477, 213
 Clausen J. V., Torres G., Bruntt H., Andersen J., Nordström B., Stefanik R. P., Latham D. W., Southworth J., 2008, *A&A*, 487, 1095
 D'Antona F., Mazzitelli I., 1991, in Michaud G., Tutukov A. V., eds, *Proc. IAU Symp. Vol. 145, Evolution of Stars: the Photospheric Abundance Connection*. Kluwer, Dordrecht, p. 399
 De Gennaro S., von Hippel T., Winget D. E., Kepler S. O., Nitta A., Koester D., Althaus L., 2008, *AJ*, 135, 1
 De Rosa R. J. et al., 2014, *MNRAS*, 437, 1216
 Delfosse X. et al., 2004, in Hilditch R. W., Hensberge H., Pavlovski K., eds, *ASP Conf. Ser. Vol. 318, Spectroscopically and Spatially Resolving the Components of the Close Binary Stars*. Astron. Soc. Pac., San Francisco, p. 166
 Dobbie P. D., Kenyon F., Jameson R. F., Hodgkin S. T., Hambly N. C., Hawkins M. R. S., 2002, *MNRAS*, 329, 543
 Dobbie P. D. et al., 2006a, *MNRAS*, 369, 383
 Dobbie P. D., Napiwotzki R., Lodieu N., Burleigh M. R., Barstow M. A., Jameson R. F., 2006b, *MNRAS*, 373, L45
 Dobbie P. D., Napiwotzki R., Burleigh M. R., Williams K. A., Sharp R., Barstow M. A., Casewell S. L., Hubeny I., 2009, *MNRAS*, 395, 2248
 Dobbie P. D., Baxter R., Külebi B., Parker Q. A., Koester D., Jordan S., Lodieu N., Euchner F., 2012a, *MNRAS*, 421, 202
 Dobbie P. D., Day-Jones A., Williams K. A., Casewell S. L., Burleigh M. R., Lodieu N., Parker Q. A., Baxter R., 2012b, *MNRAS*, 423, 2815
 Dobbie P. D. et al., 2013, *MNRAS*, 428, L16
 Duquennoy A., Mayor M., 1991, *A&A*, 248, 485
 Eldridge J. J., Tout C. A., 2004, *Mem. Soc. Astron. Ital.*, 75, 694
 Ferrario L., Vennes S., Wickramasinghe D. T., Bailey J. A., Christian D. J., 1997, *MNRAS*, 292, 205
 Ferrario L., Wickramasinghe D., Liebert J., Williams K. A., 2005, *MNRAS*, 361, 1131
 Finley D. S., Koester D., 1997, *ApJ*, 489, L79
 Fischer D. A., Marcy G. W., 1992, *ApJ*, 396, 178
 Fontaine G., Brassard P., Bergeron P., 2001, *PASP*, 113, 409
 García-Berro E. et al., 2012, *ApJ*, 749, 25
 Gianninas A., Bergeron P., Ruiz M. T., 2011, *ApJ*, 743, 138

- Gil-Pons P., García-Berro E., José J., Hernanz M., Truran J. W., 2003, *A&A*, 407, 1021
- Girardi L., Bressan A., Bertelli G., Chiosi C., 2000, *A&AS*, 141, 371
- Girven J., Gänsicke B. T., Külebi B., Steeghs D., Jordan S., Marsh T. R., Koester D., 2010, *MNRAS*, 404, 159
- Hambly N. C., Davenhall A. C., Irwin M. J., MacGillivray H. T., 2001, *MNRAS*, 326, 1315
- Hambly N. C. et al., 2008, *MNRAS*, 384, 637
- Harris H. C. et al., 2003, *AJ*, 126, 1023
- Hewett P. C., Warren S. J., Leggett S. K., Hodgkin S. T., 2006, *MNRAS*, 367, 454
- Hodgkin S. T., Irwin M. J., Hewett P. C., Warren S. J., 2009, *MNRAS*, 394, 675
- Høg E. et al., 2000, *A&A*, 355, L27
- Holberg J. B., Bergeron P., 2006, *AJ*, 132, 1221
- Holberg J. B., Sion E. M., Oswald T., McCook G. P., Foran S., Subasavage J. P., 2008, *AJ*, 135, 1225
- Holberg J. B., Oswald T. D., Sion E. M., Barstow M. A., Burleigh M. R., 2013, *MNRAS*, 435, 2077
- Huang S. S., Struve O., 1956, *AJ*, 61, 300
- Iben I., Jr, 2000, in Kastner J. H., Soker N., Rappaport S., eds, *ASP Conf. Ser. Vol. 199, Asymmetrical Planetary Nebulae II: From Origins to Microstructures*. Astron. Soc. Pac., San Francisco, p. 107
- Jeffreys H., 1961, *Theory of Probability*, 3rd edn. Oxford Univ. Press, Oxford
- Jordan S., 2008, *Astron. Nachr.*, 329, 875
- Jordan S. et al., 1998, *A&A*, 330, 277
- Kalirai J. S., Richer H. B., 2010, *Phil. Trans. R. Soc. A*, 368, 755
- Kalirai J. S., Hansen B. M. S., Kelson D. D., Reitzel D. B., Rich R. M., Richer H. B., 2008, *ApJ*, 676, 594
- Kass R. E., Raftery A. E., 1995, *J. Am. Stat. Assoc.*, 90, 773
- Keller S. C. et al., 2007, *Proc. Astron. Soc. Aust.*, 24, 1
- Kepler S. O., Kleinman S. J., Nitta A., Koester D., Castanheira B. G., Giovannini O., Costa A. F. M., Althaus L., 2007, *MNRAS*, 375, 1315
- Kepler S. O. et al., 2013, *MNRAS*, 429, 2934
- Kirkpatrick J. D. et al., 2012, *ApJ*, 753, 156
- Kleinman S. J. et al., 2004, *ApJ*, 607, 426
- Kleinman S. J. et al., 2013, *ApJS*, 204, 5
- Koester D., 2010, *Mem. Soc. Astron. Ital.*, 81, 921
- Koester D., Kompa E., 2007, *A&A*, 473, 239
- Koester D., Voss B., Napiwotzki R., Christlieb N., Homeier D., Lisker T., Reimers D., Heber U., 2009, *A&A*, 505, 441
- Kouwenhoven M. B. N., Brown A. G. A., Zinnecker H., Kaper L., Portegies Zwart S. F., 2005, *A&A*, 430, 137
- Kouwenhoven M. B. N., Brown A. G. A., Portegies Zwart S. F., Kaper L., 2007, *A&A*, 474, 77
- Kowalski P. M., Saumon D., 2006, *ApJ*, 651, L137
- Kraus A. L., Hillenbrand L. A., 2007, *AJ*, 134, 2340
- Külebi B., Jordan S., Nelan E., Bastian U., Altmann M., 2010, *A&A*, 524, A36
- Lada C. J., 2006, *ApJ*, 640, L63
- Lampton M., Margon B., Bowyer S., 1976, *ApJ*, 208, 177
- Lawrence A. et al., 2007, *MNRAS*, 379, 1599
- Liebert J., Bergeron P., Holberg J. B., 2005, *ApJS*, 156, 47
- Liebert J., Fontaine G., Young P. A., Williams K. A., Arnett D., 2013, *ApJ*, 769, 7
- Limoges M.-M., Bergeron P., Dufour P., 2009, *ApJ*, 696, 1461
- McCook G. P., Sion E. M., 1999, *ApJS*, 121, 1
- McMahon R., 2012, in *Science from the Next Generation Imaging and Spectroscopic Surveys: The VISTA Hemisphere Survey (VHS) Science Goals and Status*, available at: <http://www.eso.org/sci/meetings/2012/surveys2012/program.html>
- Mamajek E. E., Hillenbrand L. A., 2008, *ApJ*, 687, 1264
- Marsh T. R., Dhillon V. S., Duck S. R., 1995, *MNRAS*, 275, 828
- Mason B. D., Gies D. R., Hartkopf W. I., Bagnuolo W. G., Jr, ten Brummelaar T., McAlister H. A., 1998, *AJ*, 115, 821
- Maxted P. F. L., Burleigh M. R., Marsh T. R., Bannister N. P., 2002, *MNRAS*, 334, 833
- Maxted P. F. L., Marsh T. R., Morales-Rueda L., Barstow M. A., Dobbie P. D., Schreiber M. R., Dhillon V. S., Brinkworth C. S., 2004, *MNRAS*, 355, 1143
- Miszalski B., Acker A., Moffat A. F. J., Parker Q. A., Udalski A., 2009, *A&A*, 496, 813
- Monet D. G. et al., 2003, *AJ*, 125, 984
- Mukadam A. S. et al., 2004, *ApJ*, 607, 982
- Napiwotzki R., Green P. J., Saffer R. A., 1999, *ApJ*, 517, 399
- Noguchi T., Maehara H., Kondo M., 1980, *Ann. Tokyo Astron. Obs.*, 18, 55
- Nordhaus J., Wellons S., Spiegel D. S., Metzger B. D., Blackman E. G., 2011, *Proc. Natl. Acad. Sci.*, 108, 3135
- Nordstroem B., Andersen J., Andersen M. I., 1996, *A&AS*, 118, 407
- Oswalt T. D., Hintzen P. M., Luyten W. J., 1988, *ApJS*, 66, 391
- Oswalt T. D., Smith J. A., Wood M. A., Hintzen P., 1996, *Nature*, 382, 692
- Parker R. J., Reggiani M. M., 2013, *MNRAS*, 432, 2378
- Parsons S. G., Marsh T. R., Gänsicke B. T., Schreiber M. R., Bours M. C. P., Dhillon V. S., Littlefair S. P., 2013, *MNRAS*, 436, 241
- Patience J., Ghez A. M., Reid I. N., Matthews K., 2002, *AJ*, 123, 1570
- Pinfield D. J., Dobbie P. D., Jameson R. F., Steele I. A., Jones H. R. A., Katsiyannis A. C., 2003, *MNRAS*, 342, 1241
- Raghavan D. et al., 2010, *ApJS*, 190, 1
- Rebassa-Mansergas A., Nebot Gómez-Morán A., Schreiber M. R., Gänsicke B. T., Schwöpe A., Gallardo J., Koester D., 2012, *MNRAS*, 419, 806
- Reid I. N., 1996, *AJ*, 111, 2000
- Reid I. N., Gizis J. E., 1997, *AJ*, 113, 2246
- Roeser S., Demleitner M., Schilbach E., 2010, *AJ*, 139, 2440
- Sana H., Gosset E., Nazé Y., Rauw G., Linder N., 2008, *MNRAS*, 386, 447
- Schlegel D. J., Finkbeiner D. P., Davis M., 1998, *ApJ*, 500, 525
- Schneider D. P. et al., 2010, *AJ*, 139, 2360
- Shafer R. A., 1991, *XSPEC, An X-ray Spectral Fitting Package, User's Guide, Version 2*, ESA TM-09. ESA, Noordwijk
- Shanks T., Metcalfe N., 2012, in *Science from the Next Generation Imaging and Spectroscopic Surveys: VST ATLAS: Science Goals and Status*, available at: <http://www.eso.org/sci/meetings/2012/surveys2012/program.html>
- Siess L., 2007, *A&A*, 476, 893
- Struve F. G. W., 1852, *Stellarum fixarum imprimis duplicium et multiplicium positiones mediae pro epocha 1830*, 0. Typ. Academica, Petropoli, CCLIII, 380 pp.; in folio; DCCC.fe.7
- Tokovinin A. A., 1997, *A&AS*, 124, 75
- Tout C. A., Wickramasinghe D. T., Liebert J., Ferrario L., Pringle J. E., 2008, *MNRAS*, 387, 897
- Tremblay P., Bergeron P., 2009, *ApJ*, 696, 1755
- Tremblay P., Bergeron P., Gianninas A., 2011, *ApJ*, 730, 128
- van Dokkum P. G., 2001, *PASP*, 113, 1420
- Vennes S., Thejll P. A., Galvan R. G., Dupuis J., 1997, *ApJ*, 480, 714
- Vennes S., Smith R. J., Boyle B. J., Croom S. M., Kawka A., Shanks T., Miller L., Loaring N., 2002, *MNRAS*, 335, 673
- Wegg C., Phinney E. S., 2012, *MNRAS*, 426, 427
- Wegner G., McMahan R. K., Boley F. I., 1987, *AJ*, 94, 1271
- Weidemann V., 2000, *A&A*, 363, 647
- Wesemael F. et al., 1994, *ApJ*, 429, 369
- Wickramasinghe D. T., Ferrario L., 2005, *MNRAS*, 356, 1576
- Williams K. A., Bolte M., Koester D., 2009, *ApJ*, 693, 355
- Yoon S.-C., Podsiadlowski P., Rosswog S., 2007, *MNRAS*, 380, 933
- York D. G. et al., 2000, *AJ*, 120, 1579
- Yuan J. W., 1992, *A&A*, 261, 105
- Zacharias N., Finch C. T., Girard T. M., Henden A., Bartlett J. L., Monet D. G., Zacharias M. I., 2013, *AJ*, 145, 44
- Zhao J. K., Oswald T. D., Willson L. A., Wang Q., Zhao G., 2012, *ApJ*, 746, 144
- Zheng Z., 1998, in *Nédellec C., Rouveirol C., eds, Proc 10th European Conference on Machine Learning, Naive Bayesian Classifier Committees*. Springer, Chemnitz, p. 196
- Zinnecker H., 1984, *Ap&SS*, 99, 41

This paper has been typeset from a $\text{\TeX}/\text{\LaTeX}$ file prepared by the author.